Sampling Schemes for Multidimensional Signals with Finite Rate of Innovation

Pancham Shukla*, *Student Member, IEEE,* and Pier Luigi Dragotti, *Member, IEEE*

SP EDICS: DSP-WAVL (Wavelets theory and applications),
DSP-SAMP (Sampling, extrapolation, and interpolation), and DSP-RECO (Signal reconstruction)

Abstract

Consider the problem of sampling signals that are nonbandlimited but have finite number of degrees of freedom per unit of time and call this number the rate of innovation. Streams of Diracs and piecewise polynomials are the examples of such signals, and thus are known as signals with finite rate of innovation (FRI) [3]. We know that the classical ('bandlimited-sinc') sampling theory does not enable perfect reconstruction of such signals from their samples since they are not bandlimited. However, the recent results on FRI sampling [3], [4] suggest that it is possible to sample and perfectly reconstruct such nonbandlimited signals using a rich class of kernels.

In this paper, we extend the results of [4] in higher dimensions using compactly supported kernels that reproduce polynomials (satisfy Strang-Fix conditions). In fact, the polynomial reproduction property of the kernel makes it possible to obtain the continuous-moments of the signal from its samples. Using these moments and the annihilating filter method (Prony's method), the innovative part of the signal, and therefore, the signal itself is perfectly reconstructed. In particular, we present local (directional derivatives based) and global (complex-moments, Radon transform based) sampling schemes for classes of FRI signals such as sets of Diracs, bilevel and planar polygons, quadrature domains (e.g. circles, ellipses, cardioids), 2-D polynomials with polygonal boundaries, and n-dimensional Diracs and convex polytopes.

This research has been promisingly explored in super-resolution algorithms [5] and distributed compression [6], and might find its applications in photogrammetry, computer graphics, and machine vision.

Manuscript received Aug 14, 2006; revised Nov 21, 2006; accepted 27 Nov 2006. This work was supported by the Engineering and Physical Sciences Research Council (EPSRC) of UK under the grant GR/S57631/01. The material of this paper was presented in part at the IEEE Int. Conf. on Image Processing (ICIP05), Genova, Italy, Sep 2005 [1], and at ICIP06, Atlanta, USA, Oct 2006 [2].

Corresponding author: Pancham Shukla is with the Communications and Signal Processing Group, Department of Electrical and Electronic Engineering, Imperial College London, London SW7 2AZ, UK (e-mail: spancham@yahoo.com, p.shukla@imperial.ac.uk).

Pier Luigi Dragotti is with the Communications and Signal Processing Group, Department of Electrical Engineering, Imperial College London, London SW7 2AZ, UK; Tel: +44 (0)20 7594 6192; Fax: +44 (0)20 7594 6234 (e-mail: p.dragotti@imperial.ac.uk).

I. INTRODUCTION

Sampling plays an important role in modern signal processing and communication applications. Shannon's classical sampling theory and its extensions are very powerful and have been extensively utilized for bandlimited signals [7], [8]. Moreover, the classical sampling is also extended to the classes of non-bandlimited signals that reside in a shift-invariant subspace [9], [8]. For a comprehensive account on the modern sampling developments, we refer to [7], [8].

Recently, novel sampling schemes have been presented for larger classes of 1-D signals that are neither bandlimited nor reside in a fixed subspace. Such signals enjoy a finite number of degrees of freedom (or rate of innovation) and are classified as signals with Finite Rate of Innovation (FRI) [3]. Streams of Diracs, nonuniform splines, and piecewise polynomials are examples of such signals. The key feature of [3] is perfect reconstruction of FRI signals from a finite number of samples using annihilating filter method (Prony's method). Subsequently, the schemes of [3] are extended for the classes of 2-D FRI signals such as sets of 2-D Diracs, and polygons in [10] and [11]. The schemes of [10] rely on global algorithms in Fourier domain, and can be unstable at times. Most importantly, all these schemes [3], [10], [11] use infinite support sinc and Gaussian kernels, and therefore, are not convenient in practice. However, the results of [12], [4] show that many 1-D FRI signals with local rate of innovation can be sampled and perfectly reconstructed using compactly supported kernels (e.g. B-splines [13]) that satisfy Strang-Fix conditions [14], and therefore, reproduce polynomials.

In this paper, we extend the results of [12], [4] for multidimensional FRI signals using local kernels that reproduce polynomials. It is important to remember that the polynomial reproduction property of kernels plays a pivotal role in our sampling schemes. In particular, it allows us to obtain the moments of the signals from their samples, and using these moments the signals are reconstructed. In this paper, we propose local and global reconstruction schemes with varying degrees of complexities. Our schemes are based on three different approaches:

1) *Directional derivatives based approach:* This is a local approach for reconstructing a planar polygon from its corner points. It uses a link between continuous domain directional derivatives and discrete domain directional differences based on the fundamentals of lattice theory [15], [16], [17].
2) *Complex-moments based approach:* In this global approach, we exploit complex-moments and show that it is possible to reconstruct bilevel-convex polygons, sets of 2-D Diracs, polygonal lines, and quadrature domains (e.g. ellipses, cardioids, and lemniscates) from their samples. Implicitly, we derive a sampling perspective to the 'shape from moments method' of [18], [19], [20].

3) *Tomographic approach:* Finally, in the third approach, we integrate the moment property of Radon transform [19] in the framework of FRI sampling and derive an Annihilating-Filter-based-Back-Projection (AFBP) algorithm, which allows us to sample more general FRI signals such as 2-D polynomials with polygonal boundaries.

We show that, using these approaches, classes of multidimensional FRI signals can be sampled and perfectly reconstructed from their samples. It is important to note that we concentrate on sampling and perfect reconstruction theory, and therefore, throughout the paper we consider noiseless signals and measurements.

The paper is organized as follows: In the following section, we begin with the framework for sampling FRI signals, and introduce a local reconstruction scheme for 2-D Diracs. In Section III, we extend the local reconstruction of 2-D Diracs for planar polygons using directional derivatives based approach. We then show in Section IV that the complex-moments can be used to derive global algorithms for sampling sets of 2-D Diracs, bilevel and convex polygons, and quadrature domains. Finally, in Section V, we employ multidimensional Radon transform and AFBP algorithm for sampling more general FRI signals such as 2-D polynomials with polygonal boundaries. The concluding remarks are given in Section VI.

II. 2-D Sampling Framework

In this section, we review the concept of signals with finite rate of innovation (FRI), and describe the sampling setup and sampling kernels that we employ for the proposed schemes. We review an important tool: 'annihilating filter method' [3] which is used extensively in subsequent sections. Finally, we close this section by introducing a local reconstruction scheme for 2-D Diracs in order to demonstrate the role of polynomial reproduction in FRI sampling.

A. FRI Signals

Consider a 1-D signal of the form [3]

$$g(t) = \sum_{i=0}^{N} \sum_{n \in \mathbb{Z}} \lambda_{i,n} \, \phi_i \left(t - t_n \right), \tag{1}$$

where the set of functions $\{\phi_i(t)\}, i = 0, 1, \ldots, N$ is known. Notice that the free parameters (degrees of freedom) of $g(t)$ are the time instants t_n and coefficients $\lambda_{i,n}$.

It is therefore natural to introduce a counting function $C_g(t_a, t_b)$ that counts the number of free parameters of $g(t)$ over an interval $\tau = [t_a, t_b]$. The rate of innovation of $g(t)$ is then defined as [3]

$$\rho = \lim_{\tau \to \infty} \frac{1}{\tau} C_g \left(-\frac{\tau}{2}, \frac{\tau}{2} \right). \tag{2}$$

Definition 1 [3]: A signal with a finite rate of innovation is a signal that is characterized by (1) and with a finite ρ as given in (2).

Moreover, the notion of FRI can be extended in 2-D (or in higher dimensions). In particular, a 2-D FRI signal $g(x, y)$ is given by

$$g(x,y) = \sum_{i=0}^{N} \sum_{j \in \mathbb{Z}} \sum_{k \in \mathbb{Z}} \lambda_{i,j,k} \, \phi_i \left(x - x_j, y - y_k \right), \tag{3}$$

where the free parameters, in this case, are the shifts x_j and y_k and the coefficients $\lambda_{i,j,k}$. The local rate of innovation is then given by $\rho_{xy} = \frac{1}{\tau_x \tau_y} \, C_g \left[(-\frac{\tau_x}{2}, \frac{\tau_x}{2}), (-\frac{\tau_y}{2}, \frac{\tau_y}{2}) \right]$ over the window of size $\tau_x \times \tau_y$.

For instance, when $\phi_i \left(x, y \right) = \delta_{xy}(x, y)$, and both $x_j - x_{j-1}$ and $y_k - y_{k-1}$ are i.i.d. random variables with exponential density, then $g(x, y)$ describes a separable 2-D Poisson process. A set of 2-D Diracs is one particular realization of the 2-D Poisson process. Other examples of 2-D FRI signals include lines in 2-D, polygonal lines, convex and bilevel polygons, and classes of algebraic curves (e.g. ellipses, cardioids, and lemniscates) [10], [18].

B. Sampling Setup

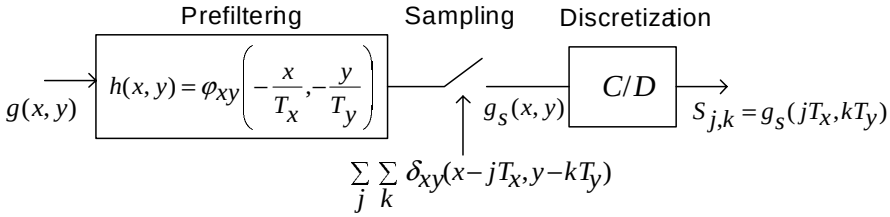

Fig. 1. A generic 2-D sampling setup: Continuous signal $g(x, y)$ is convolved by a smoothing kernel $\varphi_{xy}(x, y)$ and then sampled uniformly by $\sum_{j \in \mathbb{Z}} \sum_{k \in \mathbb{Z}} \delta_{xy}(x - jT_x, y - kT_y)$ to obtain the sampled signal $g_s(x, y)$. The block C/D represents continuous to discrete transformation and corresponds to the read-out of sample values $S_{j,k}, \; j, k \in \mathbb{Z}$ from $g_s(x, y)$.

We consider a 2-D generic sampling setup as shown in Figure 1, where a continuous 2-D FRI signal $g(x, y)$ is prefiltered by a smoothing (sampling) kernel $h(x, y) = \varphi_{xy}(-x/T_x, -y/T_y)$, and the filtered version $g(x, y) * \varphi_{xy}(-x/T_x, -y/T_y)$ is sampled uniformly to obtain the set of samples $S_{j,k}$ given by

$$\begin{aligned} S_{j,k} &= \langle g(x,y), \varphi_{xy}(x/T_x - j, y/T_y - k) \rangle \\ &= \int \int_{\mathbb{R}^2} g(x,y) \; \varphi_{xy}(x/T_x - j, y/T_y - k) \, dx \, dy, \end{aligned} \tag{4}$$

where $T_x, T_y \in \mathbb{R}^+$ are sampling intervals along x and y directions respectively. For simplicity, we assume $T_x = T_y = 1$ unless explicitly specified. Note that the setup of Figure 1 is typical for acquisition devices and processing algorithms, and can be extended to higher dimensions (i.e. in 3-D and above) [8].

C. Sampling Kernels and their Properties

It is always desirable to have a freedom in selecting or designing a sampling kernel $\varphi_{xy}(x, y)$ of choice. However, in practice, the kernel results from the physical properties of a given acquisition device and does not allow desired flexibility. Recall that the Shannon's sampling theorem uses infinite support sinc kernel (ideal low-pass filter), while the FRI schemes of [3], [10], [11] use infinite support sinc and Gaussian kernels, and for that reason, are not convenient in practice.

For the proposed sampling schemes, we consider any compactly supported kernel that satisfies Strang-Fix conditions [14] and therefore reproduces polynomials up to certain degree n. To be more precise, our sampling kernel $\varphi_{xy}(x, y)$ is given by the tensor product of two 1-D functions $\varphi(x)$ and $\varphi(y)$ that can reproduce polynomials x^α and y^β respectively, where $\alpha, \beta \in \{0, 1, \ldots, n\}$ and $x, y \in \mathbb{R}$. This means that there exists coefficients $C_{j,k}^{\alpha,\beta}$ such that the kernel $\varphi_{xy}(x, y)$ satisfies:

$$\sum_{j=-\infty}^{\infty} \sum_{k=-\infty}^{\infty} C_{j,k}^{\alpha,\beta}\, \varphi_{xy}(x - j, y - k) \quad = \quad x^\alpha\, y^\beta, \tag{5}$$

where α, β specify the degrees of polynomials that the kernel $\varphi_{xy}(x, y)$ can reproduce along x and y directions respectively. For instance, B-spline of order n can reproduce polynomial up to degree n, i.e. $\alpha, \beta \in \{0, 1, \ldots, n\}$. Notice that $C_{j,k}^{\alpha,0}$ is responsible for the reproduction of a polynomial of degree α along x-axis, while $C_{j,k}^{0,\beta}$ is responsible for the reproduction of a polynomial of degree β along y-axis.

Furthermore, for $\alpha = \beta = 0$, if the kernel $\varphi_{xy}(x, y)$ allows $C_{j,k}^{\alpha,\beta} = C_{j,k}^{0,0} = 1$, then (5) reduces to

$$\sum_{j=-\infty}^{\infty} \sum_{k=-\infty}^{\infty} \varphi_{xy}(x - j, y - k) = 1. \tag{6}$$

Above equation states that the sum of shifted versions of sampling kernel produces unit amplitude polynomial of degree zero, and is often acknowledged as 'partition of unity' in wavelet community.

Notice that the orthogonal Daubechies scaling functions [21] and biorthogonal B-splines [13] satisfy the properties of (6) and (5) and therefore are valid sampling kernels. A simple illustration of partition of unity and polynomial reproduction using B-spline sampling kernel is given in Figure 2.

D. Annihilating Filter Method

The annihilating filter method plays an important role in reconstruction of FRI signals [3]. Seeing its immediate relevance in following sections, we briefly discuss its core formulation. For in-depth treatment, we recommend [3] and [22]. This method (often termed as Prony's method) is well known in error-correction coding [23] and spectral estimation [22]. In spectral estimation, it is common to observe a signal $\tau[n]$ that is composed of linear combinations of exponentials such that

$$\tau[n] = \sum_{i=0}^{N-1} \rho_i \, u_i^n, \quad \rho_i \in \mathbb{C}, u_i \in \mathbb{C}, n \in \mathbb{N}, \tag{7}$$

where ρ_i denotes weights, and u_i denotes locations of the spectral components.

The annihilating filter method consists of two steps:

1) Design of the filter $A[n]$ that annihilates signal $\tau[n]$, that is $A[n] * \tau[n] = 0, \ \forall \, n \in N$.
2) Determination of the locations u_i and weights ρ_i using filter $A[n]$ and observed signal $\tau[n]$.

Consider the signal $\tau[n]$ of (7), and a filter $A[n], \ n = 0, 1, \ldots, N$ with z-transform

$$A(z) = \sum_{n=0}^{N} A[n] \, z^{-n} = \prod_{i=0}^{N-1} \left(1 - u_i \, z^{-1}\right), \tag{8}$$

where u_i's are distinct. It then follows that

$$\begin{aligned} A[n] * \tau[n] &= \sum_{l=0}^{N} A[l] \, \tau[n-l] && (9) \\ &= \sum_{l=0}^{N} \sum_{i=0}^{N-1} \rho_i \, A[l] \, u_i^{n-l} \\ &= \sum_{i=0}^{N-1} \rho_i \underbrace{\left(\sum_{l=0}^{N} A[l] \, u_i^{-l} \right)}_{=0 \text{ from } (8)} u_i^n \\ &= 0. && (10) \end{aligned}$$

Thus, the filter $A[n]$ is called annihilating filter since it annihilates the observed signal $\tau[n]$. Notice that $A[n]$ is unique for the observed signal $\tau[n]$, since the u_i's are distinct. Clearly, the knowledge of $A[n]$ is sufficient to retrieve the locations $u_0, u_1, \ldots, u_{N-1}$, since these locations are the roots of filter $A(z)$ in (8).

Since there are N unknown coefficients of $A[n]$ (recall that $A[0] = 1$), we need to solve a system of N linear equations, and therefore, require at least $2N$ values of $\tau[n]$. For instance, the observations $\tau[0], \tau[1], \ldots, \tau[2N-1]$

allow to describe the convolution $A[n] * \tau[n] = 0$ in matrix/vector form as:

$$\begin{bmatrix} \tau[N-1] & \tau[N-2] & \cdots & \tau[0] \\ \tau[N] & \tau[N-1] & \cdots & \tau[1] \\ \vdots & \vdots & \ddots & \vdots \\ \tau[2N-2] & \tau[2N-3] & \cdots & \tau[N-1] \end{bmatrix} \begin{bmatrix} A[1] \\ A[2] \\ \vdots \\ A[N] \end{bmatrix} = - \begin{bmatrix} \tau[N] \\ \tau[N+1] \\ \vdots \\ \tau[2N-1] \end{bmatrix}. \tag{11}$$

The solution of this Yule-Walker system gives the filter coefficients $A[n]$. From equation (8), it is straightforward to see that the roots of filter $A(z)$ are the locations u_i.

Once the locations u_i are known, the weights ρ_i are determined by solving equation (7) as follows

$$\begin{bmatrix} 1 & 1 & \cdots & 1 \\ u_0 & u_1 & \cdots & u_{N-1} \\ \vdots & \vdots & \ddots & \vdots \\ u_0^{N-1} & u_1^{N-1} & \cdots & u_{N-1}^{N-1} \end{bmatrix} \begin{bmatrix} \rho_0 \\ \rho_1 \\ \vdots \\ \rho_{N-1} \end{bmatrix} = \begin{bmatrix} \tau[0] \\ \tau[1] \\ \vdots \\ \tau[N-1] \end{bmatrix}. \tag{12}$$

Given that all locations u_i are distinct, the Vandermonde system of (12) is invertible and yields a unique solution for the weights ρ_i.

Moreover, it is possible to show that the signals of form $\tau[n] = \sum_{i=0}^{N-1} \rho_i \, n^R \, u_i^n$ are annihilated by the filter $A(z) = \prod_{i=0}^{N-1} \left(1 - u_i z^{-1}\right)^{R+1}$ [3]. This method has been successfully utilized for determining weights ρ_i and locations u_i of the streams of differentiated Diracs, and therefore, for the reconstruction of piecewise polynomial signals [3], [12], [4].

E. Local Reconstruction of 2-D Diracs

Now to demonstrate the essential role of polynomial reproduction in the proposed FRI sampling, we begin with a simple class of FRI signals. Consider a set of 2-D Diracs $g(x,y) = \sum_{i \in \mathbb{Z}} a_i \, \delta_{xy}\left(x - x_i, y - y_i\right)$, $a, x, y \in \mathbb{R}$. It is important to note that each 2-D Dirac can be parameterized by an amplitude a_i and a coordinate position (x_i, y_i), and thus has a finite number of degrees of freedom (or rate of innovation) which equals three.

We observe the samples $S_{j,k} = \langle g(x,y), \varphi_{xy}(x/T_x - j, y/T_y - k) \rangle$, where T_x, T_y are the sampling intervals and $\varphi_{xy}(x,y)$ is the sampling kernel with compact support $L_x \times L_y$. Assume that the Diracs in signal $g(x,y)$ are distributed in such a way that there is at most one Dirac in any given window of size $(L_x+1)T_x \times (L_y+1)T_y$ and assume that the kernel $\varphi_{xy}(x,y)$ can reproduce polynomials up to degree one, i.e. $\alpha, \beta \in \{0,1\}$ in (5). Therefore, from (6), an algebraic sum of shifted kernels is constant and equals to unity (see Figure 2 (b)). Whereas from (5),

the linear combinations of shifted kernels with coefficients $C_{j,k}^{1,0}$ and $C_{j,k}^{0,1}$ produce unit-slope linear functions along x and y directions (see Figures 2 (c) and (d)). Moreover with above assumptions, we are sure that only $L_x \times L_y$ inner products (or samples) $S_{j,k} = \langle g(x,y), \varphi_{xy}(x/T_x - j, y/T_y - k) \rangle$ overlap in an arbitrary window of size $(L_x+1)T_x \times (L_y+1)T_y$ that encloses a unique Dirac $a_p\,\delta_{xy}(x - x_p, y - y_p),\ p \in \mathbb{Z}$.

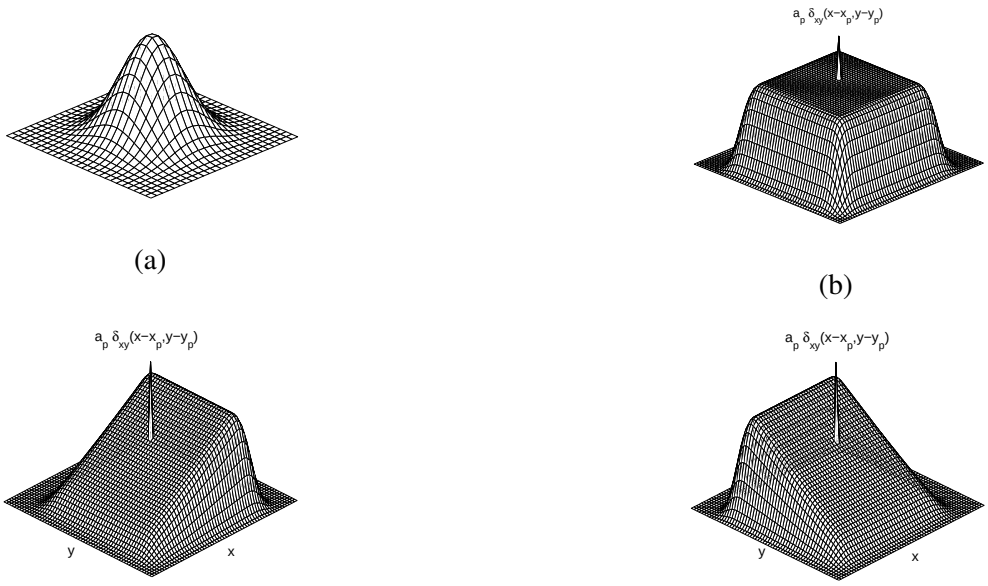

(a) (b) (c) (d)

Fig. 2. Local reconstruction of a 2-D Dirac $a_p\,\delta_{xy}(x-x_p, y-y_p)$: The B-spline sampling kernel $\beta_{xy}^3(x,y)$ that can reproduce polynomials up to degree 3 is given in part (a). The reproduction of polynomial of degree 0 (partition of unity), responsible for the determination of amplitude a_p is given in part (b), whereas the reproduction of polynomials of degree 1 along x and y directions, responsible for the determination of coordinates x_p and y_p are given in part (c) and part (d) respectively.

Therefore, for a given Dirac (assuming $T_x = T_y = 1$), it follows that

$$\begin{aligned}
\sum_{j=1}^{L_x}\sum_{k=1}^{L_y} S_{j,k} &= \left\langle a_p\delta_{xy}(x-x_p, y-y_p), \sum_{j=1}^{L_x}\sum_{k=1}^{L_y}\varphi_{xy}(x-j, y-k)\right\rangle \\
&= \int_{-\infty}^{\infty}\int_{-\infty}^{\infty} a_p\delta_{xy}(x-x_p, y-y_p)\left(\sum_{j=1}^{L_x}\sum_{k=1}^{L_y}\varphi_{xy}(x-j, y-k)\right)dx\,dy \\
&= a_p\sum_{j=1}^{L_x}\sum_{k=1}^{L_y}\varphi_{xy}(x_p-j, y_p-k) \\
&= a_p \qquad \text{(from equation (6))}
\end{aligned} \tag{13}$$

and

$$\begin{aligned}
\sum_{j=1}^{L_x}\sum_{k=1}^{L_y} C_{j,k}^{1,0}\ S_{j,k} &= \left\langle a_p\delta_{xy}(x-x_p,y-y_p), \sum_{j=1}^{L_x}\sum_{k=1}^{L_y} C_{j,k}^{1,0}\,\varphi_{xy}(x-j,y-k)\right\rangle \\
&= \int_{-\infty}^{\infty}\int_{-\infty}^{\infty} a_p\delta_{xy}(x-x_p,y-y_p)\left(\sum_{j=1}^{L_x}\sum_{k=1}^{L_y} C_{j,k}^{1,0}\,\varphi_{xy}(x-j,y-k)\right)dx\,dy \\
&= a_p\sum_{j=1}^{L_x}\sum_{k=1}^{L_y} C_{j,k}^{1,0}\,\varphi_{xy}(x_p-j,y_p-k) \\
&= a_p x_p \qquad \text{(from equation (5))}. \qquad (14)
\end{aligned}$$

Similarly, it is straightforward to arrive at $\sum_{j=1}^{L_x}\sum_{k=1}^{L_y} C_{j,k}^{0,1}\,S_{j,k} = a_p\,y_p$ in the line of above derivation.

Thus, the amplitude a_p of a given Dirac is retrieved using

$$a_p = \sum_{j=1}^{L_x}\sum_{k=1}^{L_y} S_{j,k}, \qquad (15)$$

and the position (x_p, y_p) is retrieved using

$$\begin{aligned}
x_p &= \left(\sum_{j=1}^{L_x}\sum_{k=1}^{L_y} C_{j,k}^{1,0}\ S_{j,k}\right)\Big/ a_p, \\
y_p &= \left(\sum_{j=1}^{L_x}\sum_{k=1}^{L_y} C_{j,k}^{0,1}\ S_{j,k}\right)\Big/ a_p, \qquad (16)
\end{aligned}$$

where the coefficients $C_{j,k}^{1,0}$ and $C_{j,k}^{0,1}$ are identified from equation (5).

Hence, a local reconstruction scheme for 2-D Diracs follows

Proposition 1: Assume a sampling kernel $\varphi_{xy}(x,y)$ with support $L_x \times L_y$ that can reproduce polynomials of degree zero and one along the Cartesian axes x and y. A set of finite amplitude 2-D Diracs $g(x,y) = \sum_{i\in\mathbb{Z}} a_i\,\delta_{xy}(x-x_i, y-y_i)$ is uniquely determined from its samples defined by $S_{j,k} = \langle g(x,y), \varphi_{xy}(x/T_x - j, y/T_y - k)\rangle$, if there is at most one Dirac in any distinct window of size $(L_x+1)T_x \times (L_y+1)T_y$.

III. Directional Derivatives Based Approach

The contribution of this section is two-fold: 1) We extend the local reconstruction scheme of 2-D Diracs for planar polygons and develop an algorithm useful for super-resolution corner reconstruction; 2) In developing this algorithm, we derive a link between continuous domain directional derivatives and discrete domain directional differences based on the fundamentals of lattice theory [17], which in turn, provides a background for the tomographic approach of Section V.

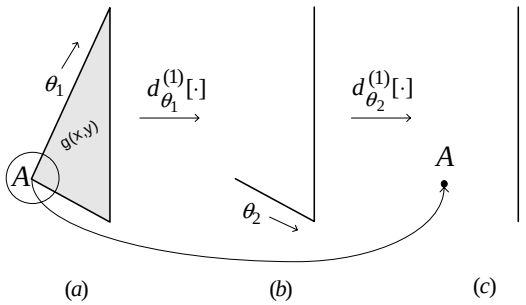

Fig. 3. For a given planar polygon $g(x, y)$, a pair of two successive first order directional derivatives $d^{(1)}_{\theta_1}[\cdot]$ and $d^{(1)}_{\theta_2}[\cdot]$ decomposes a corner point A into a 2-D Dirac.

Consider a planar polygon $g(x, y)$ with N corner points as shown in Figure 3(a). The sides of the polygon are identified by the 2-D lines:

$$y_i = \tan(\theta_i)\, x_i + b_i, \quad i = 1, 2, \ldots, N,$$

where b_i are the shifts and θ_i are the orientations.

For this N sided polygon, consider an arbitrary corner point (e.g. point A in Figure 3) formed by two sides with orientations θ_1 and θ_2. A pair of first order directional derivatives $d^{(1)}_{\theta_1}[\cdot]$ and $d^{(1)}_{\theta_2}[\cdot]$ on $g(x, y)$ can be written as

$$\begin{aligned} d^{(1)}_{\theta_2}\left[d^{(1)}_{\theta_1}[g(x,y)]\right] &= \cos(\theta_1)\cos(\theta_2)\frac{\partial^2}{\partial x^2}\Big(g(x,y)\Big) + \sin(\theta_1+\theta_2)\frac{\partial}{\partial y}\Big(\frac{\partial}{\partial x}\Big(g(x,y)\Big)\Big) + \\ &\quad \sin(\theta_1)\sin(\theta_2)\frac{\partial^2}{\partial y^2}\Big(g(x,y)\Big). \end{aligned} \tag{17}$$

Clearly, this pair of directional derivatives produces a 2-D Dirac at the corner point A (see Figures 3(b) and (c)). Likewise, we can 'turn' other corner points into Diracs by selecting proper pairs of derivatives. This suggests that the local reconstruction scheme of Diracs, described in previous section, can be tailored for reconstructing corner points of planar polygons.

However, the practical difficulty is that instead of a direct access to the polygon $g(x, y)$, we only have access to its samples $S_{j,k} = \langle g(x, y), \varphi_{xy}(x/T_x - j, y/T_y - k)\rangle$, where $\varphi_{xy}(x, y)$ is a sampling kernel that can reproduce a polynomial of degree zero. Fortunately, discrete equivalent to the directional derivatives is directional differences, and directional differences can be connected to the corresponding continuous derivatives. This connection is based on the fundamentals of lattice theory, and in particular, involves subsampling over rectangular lattices. Since we are dealing with a finite number of samples $S_{j,k}, j, k \in \mathbb{Z}$ over a uniform rectangular grid, we focus onto the 2-D integer lattices. For further details on lattice theory, we refer to [15], [16], [17].

For a given corner point, assume that the orientations θ_1 and θ_2 of the two adjacent polygonal sides are such

that $\theta_1 = \tan^{-1}\left(\frac{v_{1,2}}{v_{1,1}}\right)$ and $\theta_2 = \tan^{-1}\left(\frac{v_{2,2}}{v_{2,1}}\right)$ where $v_{1,1}, v_{1,2}, v_{2,1}, v_{2,2} \in \mathbb{Z}$. Let the corresponding base lattice Λ be given by $\Lambda = \{\lambda : \lambda = n_1\vec{v}_1 + n_2\vec{v}_2\}$, where $\vec{v}_i = [v_{i,1}, v_{i,2}]$, $i = 1, 2$ are its basis vectors. The lattice Λ is characterized by a sampling matrix $V_\Lambda = \begin{bmatrix} v_{1,1} & v_{1,2} \\ v_{2,1} & v_{2,2} \end{bmatrix}$ with determinant $\det(V_\Lambda)$.

Now compute the finite differences of the samples $S_{j,k}$, first along the lattice direction $\vec{v}_1$ and then along $\vec{v}_2$. Assuming $T_x = T_y = 1$, it then follows that

$$\begin{aligned} R_{j,k} &= \mathcal{D}^{(1)}_{\theta_2}\left[\mathcal{D}^{(1)}_{\theta_1}[S_{j,k}]\right] = \left\{S_{(j+v_{2,1}+v_{1,1}),(k+v_{2,2}+v_{1,2})} - S_{(j+v_{2,1}),(k+v_{2,2})}\right\} - \left\{S_{(j+v_{1,1}),(k+v_{1,2})} - S_{j,k}\right\} \\ &= \Big\langle g(x,y), \Big\{\varphi_{xy}\big(x-(j+v_{2,1}+v_{1,1}), y-(k+v_{2,2}+v_{1,2})\big) - \varphi_{xy}\big(x-(j+v_{2,1}), y-(k+v_{2,2})\big)\Big\} - \\ &\quad \Big\{\varphi_{xy}\big(x-(j+v_{1,1}), y-(k+v_{1,2})\big) - \varphi_{xy}\big(x-j, y-k\big)\Big\}\Big\rangle, \end{aligned}$$

and by using Parseval's identities, and after certain manipulations (refer Appendix-I), we derive that

$$\frac{R_{j,k}}{|\det(V_\Lambda)|} = \frac{\mathcal{D}^{(1)}_{\theta_2}\left[\mathcal{D}^{(1)}_{\theta_1}[S_{j,k}]\right]}{|\det(V_\Lambda)|} = \left\langle \frac{\partial}{\partial\theta_2}\Big(\frac{\partial}{\partial\theta_1}\Big(g(x,y)\Big)\Big), \zeta_{\theta_1,\theta_2}(x-j, y-k)\right\rangle, \tag{18}$$

where $\zeta_{\theta_1,\theta_2}(x,y) = \frac{\left(\varphi_{xy}(x,y) * \beta^0_{\theta_1}(x,y)\right) * \beta^0_{\theta_2}(x,y)}{|\sin(\theta_2-\theta_1)|}$ is a modified kernel, and $\beta^0_{\theta_1}(x,y)$ and $\beta^0_{\theta_2}(x,y)$ are the 1-D B-splines of order zero in xy-plane along orientations θ_1 and θ_2 respectively. For example, assuming that the original kernel $\varphi_{xy}(x,y)$ is a Haar scaling function (see Figure 4(a)), the modified kernel $\zeta_{\theta_1,\theta_2}(x,y)$ is shown in Figure 4(b). Since the skewness of the modified kernel depends on orientations θ_1 and θ_2, we denote the modified kernel as 'directional kernel'.

(a) (b)

Fig. 4. Original and directional kernels: (a) $\varphi_{xy}(x,y)$ is a Haar scaling function with support 1×1, (b) Directional kernel $\zeta_{\theta_1,\theta_2}(x,y)$ with support 4×4 for a given corner point of the polygon $g(x,y)$ formed by the two sides with orientations $\tan(\theta_1) = 2/1$ and $\tan(\theta_2) = -1/2$.

The kernel $\zeta_{\theta_1,\theta_2}(x,y)$ is of compact support $L_{x,\theta_1,\theta_2} \times L_{y,\theta_1,\theta_2} = (|v_{1,1}| + |v_{2,1}| + L_x) \times (|v_{1,2}| + |v_{2,2}| + L_y)$, where $L_x \times L_y$ is the support of the original sampling kernel $\varphi_{xy}(x,y)$. The skewed shape of kernel $\zeta_{\theta_1,\theta_2}(x,y)$, and the factors $\frac{1}{|\det(V_\Lambda)|}$ and $\frac{1}{|\sin(\theta_2-\theta_1)|}$ in equation (18) are due to subsampling over integer lattices. It is important to note that there exists an independent directional kernel $\zeta_{\theta_i,\theta_{i+1}}(x,y)$, $i = 1, 2, \ldots, N$ for each independent corner point of the polygon $g(x,y)$, where $\theta_{i+N} = \theta_i$.

Equation (18) states that the new samples $R_{j,k}$ given by the finite differences along $\vec{v}_1$ and $\vec{v}_2$ are equivalent to those obtained by sampling $d^{(1)}_{\theta_2}\left[d^{(1)}_{\theta_1}[g(x,y)]\right]$ with the directional kernel $\zeta_{\theta_1,\theta_2}(x,y)$. Moreover, if all the corner points of the polygon $g(x,y)$ are sufficiently apart such that there is at most one corner point in any distinct window of size $(L_{x,\theta_i,\theta_{i+1}}+1)T_x \times (L_{y,\theta_i,\theta_{i+1}}+1)T_y$, $i=1,2,\ldots,N$, then it is possible to reconstruct the corner points using local reconstruction scheme of 2-D Diracs as given in Section II-E.

Assuming that the kernel $\varphi_{xy}(x,y)$ satisfies partition of unity (6), the directional kernel $\zeta_{\theta_1,\theta_2}(x,y)$ always satisfies partition of unity (6) and reproduces polynomials up to degree one (5) along both x and y directions. These properties of the directional kernel $\zeta_{\theta_1,\theta_2}(x,y)$ enable us to determine the amplitude a_p and the coordinate position (x_p,y_p) of the resultant 2-D Dirac $a_p\delta_{xy}(x-x_p,y-y_p)$ at the given corner point using a finite number of samples $R_{j,k}$. In fact, we only need a small isolated group of samples (i.e. $L_{x,\theta_1,\theta_2} \times L_{y,\theta_1,\theta_2}$ samples) in the vicinity of the given corner point. Hence the local reconstruction scheme of (15) and (16), for the given corner point (e.g. point A) leads to the following identities

$$a_p = \frac{\sum_j \sum_k R_{j,k}}{|\det(V_\Lambda)|}, \tag{19}$$

$$x_p = \frac{\sum_j \sum_k C^{1,0}_{j,k}\, R_{j,k}}{a_p\,|\det(V_\Lambda)|}, \qquad y_p = \frac{\sum_j \sum_k C^{0,1}_{j,k}\, R_{j,k}}{a_p\,|\det(V_\Lambda)|}, \tag{20}$$

where $C^{1,0}_{j,k}$ and $C^{0,1}_{j,k}$ are the coefficients of kernel $\zeta_{\theta_1,\theta_2}(x,y)$, identified from equation (5).

Clearly, the coordinate pair (x_p,y_p) gives the position of the given corner point (e.g. point A), whereas a_p gives the amplitude of the planar polygon $g(x,y)$. It is straightforward to see that this reconstruction scheme applies equally to all the corner points of $g(x,y)$ using appropriate directional kernels $\zeta_{\theta_i,\theta_{i+1}}(x,y)$, $i=1,2,\ldots,N$. From the knowledge of the corner points and directions, it is possible to reconstruct the polygon $g(x,y)$. To summarize, we have

Proposition 2: Assume an N sided planar polygon $g(x,y)$ with the orientations $\theta_i, i=1,2,\ldots,N$ of its sides satisfying $\tan(\theta_i) \in \mathbb{Q}$, and that the kernel $\varphi_{xy}(x,y)$ can reproduce polynomial of at least degree zero, a set of samples $S_{j,k} = \langle g(x,y), \varphi_{xy}(x/T_x - j, y/T_y - k)\rangle$ is sufficient to reconstruct the polygon $g(x,y)$ provided that there is at most one corner point in any distinct window of size $(L_{x,\theta_i,\theta_{i+1}}+1)T_x \times (L_{y,\theta_i,\theta_{i+1}}+1)T_y$, where $L_{x,\theta_i,\theta_{i+1}} \times L_{y,\theta_i,\theta_{i+1}}$ is the support of the directional kernel $\zeta_{\theta_i,\theta_{i+1}}(x,y)$, and $\theta_{i+N}=\theta_i$.

In practice, the orientations of the polygonal sides are not known in advance. However, if we assume that the

sides of the N sided planar polygon $g(x,y)$ take only a finite number of orientations θ_i, where $\tan(\theta_i) \in \mathbb{Q}$. Then by trying all possible orientations we can retrieve the correct ones. More precisely, given a large enough set of samples $S_{j,k} = \langle g(x,y), \varphi_{xy}(x/T_x - j, y/T_y - k)\rangle$, the reconstruction of $g(x,y)$ is realized by the following steps.

Algorithm- Reconstruction of planar polygon using directional derivatives

1) Apply a distinct pair of finite differences $\mathcal{D}^{(1)}_{\theta_1}[\cdot]$ and $\mathcal{D}^{(1)}_{\theta_2}[\cdot]$ over the set of samples $S_{j,k}$ and obtain a new set of samples $R_{j,k} = \mathcal{D}^{(1)}_{\theta_2}\left[\mathcal{D}^{(1)}_{\theta_1}[S_{j,k}]\right]$.
2) Check whether at least one isolated group of samples in $R_{j,k}$ is segmented. If yes, then using the local reconstruction scheme of (19) and (20), determine the amplitude a_p and the position (x_p, y_p) of the Dirac, and therefore, the corner point.
3) Reiterate from step 1 (with a new pair) until all N corner points are determined.
4) Using the recovered corner points and the successful pairs of orientations, reconstruct the polygon $g(x,y)$.

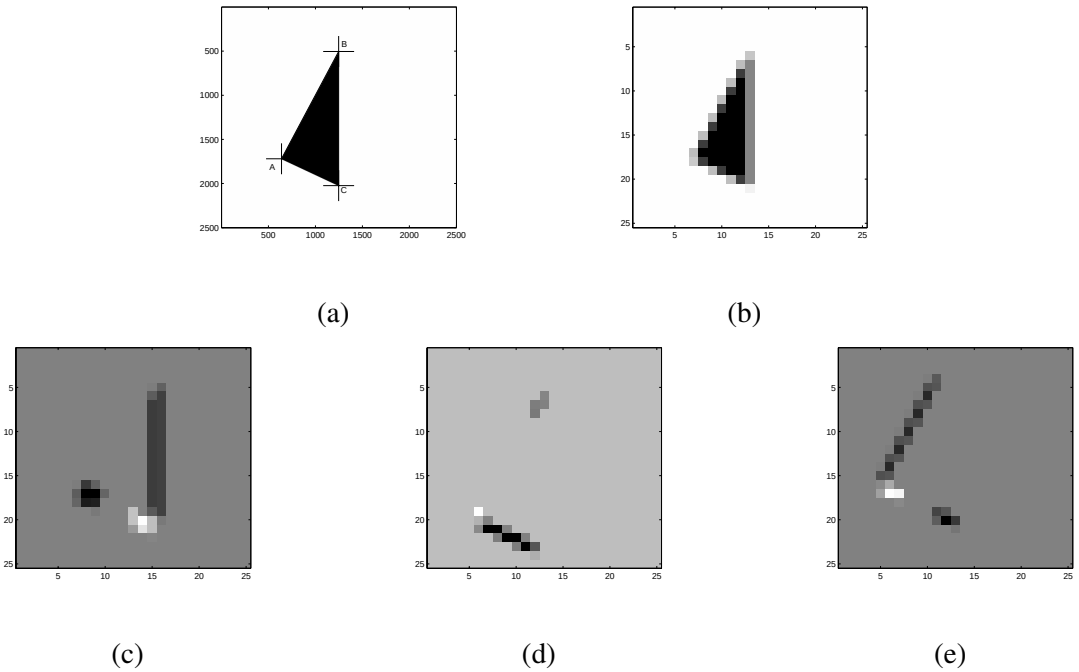

Fig. 5. Simulation result for the planar triangle $g(x,y)$ with three corner points A, B, and C such that its sides AB, BC, and CA are oriented at $\tan(\theta_1) = 2$, $\tan(\theta_3) = -\infty$, and $\tan(\theta_2) = -\frac{1}{2}$ respectively: The original image of size 2500×2500 pixels as given in part (a) is filtered with the Haar kernel $\varphi_{xy}(x,y)$ of size 100×100, and a set of 25×25 samples $S_{j,k}$ is obtained as given in part (b). A set of new samples $R_{j,k}$ that isolates corner point A, using a pair of directional differences $\mathcal{D}^{(1)}_{\theta_1}[\cdot]$ and $\mathcal{D}^{(1)}_{\theta_2}[\cdot]$ along the sides AB and AC, is given in part (c). Similarly, other two sets of differentiated samples $R_{j,k}$ that isolate corner points B and C are given in parts (d) and (e) respectively. Using the local reconstruction scheme of (19) and (20), the reconstructed corner points A, B, and C (marked with $+$) are given in part (a).

We conclude this section with a simple numerical example. Consider the case, where $g(x,y)$ is a planar triangle

ABC with its sides AB, BC, and CA oriented along $\tan(\theta_1) = 2$, $\tan(\theta_3) = -\infty$, and $\tan(\theta_2) = -1/2$ respectively. The simulation results are shown in Figure 5. The original polygon $g(x, y)$ is given in part (a). The set of samples $S_{j,k}$ obtained using the Haar kernel is given in part (b). The new set of samples $R_{j,k} = \mathcal{D}^{(1)}_{\theta_2}\left[\mathcal{D}^{(1)}_{\theta_1}[S_{j,k}]\right]$ derived from $S_{j,k}$ using a pair of finite differences $\mathcal{D}^{(1)}_{\theta_1}[\cdot]$ and $\mathcal{D}^{(1)}_{\theta_2}[\cdot]$ is given in part (c). Similarly, the sets of samples $R_{j,k}$ obtained by the differences $\mathcal{D}^{(1)}_{\theta_3}\left[\mathcal{D}^{(1)}_{\theta_1}[S_{j,k}]\right]$ and $\mathcal{D}^{(1)}_{\theta_3}\left[\mathcal{D}^{(1)}_{\theta_2}[S_{j,k}]\right]$ are given in parts (d) and (e) respectively. The small isolated groups of samples in parts (c), (d), and (e) represent three 2-D Diracs that correspond to the corner points A, B, and C respectively. These corner points are retrieved using the local reconstruction scheme of (19) and (20) and are marked with + in Figure 5(a). The reconstruction of the corner points is exact to machine precision. The computational cost of this local reconstruction algorithm is linear with the number N of corner points, that is, of the order of $\mathcal{O}(N)$.

IV. Complex-moments Based Approach

In the previous section we have shown that planar polygons can be reconstructed locally if the corner points are sufficiently apart. In this section, we present a global scheme which includes polygons with close corner points. In particular, we show that bilevel and convex polygons, sets of Diracs, polygonal lines, and quadrature domains (e.g. ellipses, and cardioids) are perfectly reconstructed from their samples using complex-moments and annihilating filter method. Implicitly, we provide a sampling perspective to the 'shape from moments method' of [18], [20].

A. Background

The relationship between shapes and moments finds its application in many diverse fields such as computer tomography, geophysical inversion, thermal imaging, and pattern recognition [19], [20], [24]. In fact, the general formulation of recovering shapes from their moments is highly ill-posed problem [18], [20]. However, it has been shown that certain classes of shapes such as binary polygons and quadrature domains are uniquely determined by a finite number of moments [25], [18].

Formally, the geometric moments $\mu_{\alpha,\beta}$ of order $n = (\alpha + \beta)$ of a 2-D function $g(x, y)$ in the closure $\Omega \in \mathbb{R}^2$ are defined as [24], [26]

$$\mu_{\alpha,\beta} = \int\int_{\Omega} g(x, y)\, x^{\alpha}\, y^{\beta}\, dx\, dy, \tag{21}$$

where $\alpha, \beta \in \{0, 1, \ldots, n\}$. Similarly, the complex-moments $\tau_{\alpha,\beta}$ of order $n = (\alpha + \beta)$ of $g(x, y)$ are defined

as [27]

$$\tau_{\alpha,\beta} = \int\int_{\Omega} g(x,y)\,(x+iy)^{\alpha}\,(x-iy)^{\beta}\,dx\,dy, \tag{22}$$

where $i = \sqrt{-1}$. Sometimes, it is convenient to use simple complex-moment τ_n of order $n = (\alpha+\beta)$ as given by [19]

$$\tau_n = \int\int_{\Omega} g(x,y)\,(x+iy)^{n}\,dx\,dy. \tag{23}$$

Note that the binomial expansion of $(x+iy)^n$ in (23) facilitates to retrieve an nth order complex-moment τ_n from the nth order geometric moments $\mu_{\alpha,\beta}$ using:

$$\tau_n = \sum_{\beta=0}^{n} \binom{n}{\beta} i^{\beta}\,\mu_{\alpha,\beta}, \quad \text{with} \quad \alpha = n-\beta. \tag{24}$$

Now assume that we observe a sampled version of $g(x,y)$, that is, we observe samples $S_{j,k} = \langle g(x,y), \varphi_{xy}(x/T_x - j, y/T_y - k)\rangle$, where the kernel $\varphi_{xy}(x,y)$ can reproduce polynomials along x and y directions. By using polynomial reproduction property of $\varphi_{xy}(x,y)$, we can show that it is possible to retrieve the moments $\mu_{\alpha,\beta}$ of $g(x,y)$ from its samples $S_{j,k}$ accurately. In fact, we have that

$$\begin{aligned}
\mu_{\alpha,\beta} &= \int\int_{\Omega} g(x,y)\,x^{\alpha}\,y^{\beta}\,dx\,dy \\
&\overset{(a)}{=} \int\int_{\Omega} g(x,y) \sum_j \sum_k C_{j,k}^{\alpha,\beta}\,\varphi_{xy}(x-j,y-k)\,dx\,dy \\
&= \sum_j \sum_k C_{j,k}^{\alpha,\beta} \int\int_{\Omega} g(x,y)\,\varphi_{xy}(x-j,y-k)\,dx\,dy \\
&\overset{(b)}{=} \sum_j \sum_k C_{j,k}^{\alpha,\beta}\,S_{j,k},
\end{aligned} \tag{25}$$

where the equalities (a) and (b) are obtained from (5) and (4) respectively.

This result is at the heart of our sampling schemes. With the 'sample-moment' connection (25) at our disposal, we now begin with the global reconstruction of bilevel polygons.

B. Bilevel Polygons

Let $g(x,y)$ be a bilevel, simply connected, and non-degenerate polygon with N corner points (vertices) z_l, $l = 1,2,\ldots,N$ in the complex plane $z = x+iy$. For such a polygon, Davis's theorem [25] states that

$$\int\int_{\Omega} g(x,y)\,h^{(2)}(z)\,dx\,dy = \sum_{l=1}^{N} \rho_l h(z_l), \tag{26}$$

where $h(z)$ is an analytic function in a closure Ω, $h^{(2)}(z)$ is the second order derivative of $h(z)$, and ρ_l are complex coefficients.

In [19], Milanfar et al. re-examined Davis's work (26) and employed a specific analytic function $h(z) = z^n$. Assuming that the corner points z_l (with z_l^* as their complex conjugates) are arranged in counter-clockwise direction in order of increasing index and satisfy the modulo operation $z_l = z_{l+N}$, it was shown that the complex coefficients ρ_l are given by [19]:

$$\rho_l = \frac{i}{2}\left(\frac{z_{l-1}^* - z_l^*}{z_{l-1} - z_l} - \frac{z_l^* - z_{l+1}^*}{z_l - z_{l+1}}\right), \quad l = 1, 2, \ldots, N,$$

and that

$$\begin{aligned}
\sum_{l=1}^{N} \rho_l \, z_l^n &= \int\int_{\Omega} g(x,y)\, h^{(2)}(z)\, dx\, dy \\
&= \int\int_{\Omega} g(x,y)(z^n)^{(2)}\, dx\, dy \\
&= n(n-1)\int\int_{\Omega} g(x,y)(x+iy)^{n-2}\, dx\, dy \\
&= \hat{\tau}_n \quad \forall\, n \geq 2,
\end{aligned} \tag{27}$$

where $\hat{\tau}_n$ is the complex-moment with weight $n(n-1)$, and is related to the simple complex-moment τ_n of (23) by $\hat{\tau}_n = n(n-1)\tau_{n-2}$. Note that $\hat{\tau}_0 = \hat{\tau}_1 = 0$ by definition.

From equation (27), it is clear that the weighted complex-moments $\hat{\tau}_n$ are the linear combinations of exponentials z_l^n. Therefore, the annihilating filter method, described in Section II-D, can be employed to retrieve the N corner points z_l of $g(x,y)$ from the $2N$ complex-moments $\hat{\tau}_n, n = 0, 1, \ldots 2N-1$. Moreover, if the bilevel polygon $g(x,y)$ is convex, it can be uniquely reconstructed from the retrieved corner points z_l [19]. Note that the relationship among the weighted complex-moments $\hat{\tau}_n$, simplex complex-moments τ_n, and the geometric moments $\mu_{\alpha,\beta}$ facilitates to obtain the weighted complex-moments $\hat{\tau}_n$ up to order $2N-1$ from the geometric moments $\mu_{\alpha,\beta}$ of order $2N-3$.

Let us now return to the sampling setup of Figure 1, where $g(x,y)$ is a bilevel and convex polygon with N corner points $z_l = (x_l + iy_l)$, $l = 1, 2, \ldots, N$. Clearly, the rate of innovation of $g(x,y)$ is $2N$. Assume that we observe samples $S_{j,k} = \langle g(x,y), \varphi_{xy}(x/T_x - j, y/T_y - k)\rangle$ produced by the kernel $\varphi_{xy}(x,y)$ that can reproduce polynomials up to degree $2N-3$ along x and y directions. The polynomial reproduction property of $\varphi_{xy}(x,y)$ allows us to obtain the moments $\mu_{\alpha,\beta}$ of $g(x,y)$ from its samples $S_{j,k}$. Therefore, by a suitable adaption of (25) and (24) in the formulation of (27), we can obtain the complex-moments $\hat{\tau}_n$, $n = 2, 3, \ldots, 2N-1$ of $g(x,y)$ from the samples $S_{j,k}$. More precisely, the geometric moments $\mu_{\alpha,\beta}$ are given by: $\mu_{\alpha,\beta} = \sum_j \sum_k C_{j,k}^{\alpha,\beta} S_{j,k}$ with $\alpha, \beta \in \{0, 1, \ldots, 2N-3\}$ (see eq. (25)). The knowledge of $\mu_{\alpha,\beta}$ then allows us to retrieve the complex-moments τ_n using (24). Finally, the weighted complex-moments $\hat{\tau}_n$ of (27) are given by $\hat{\tau}_n = n(n-1)\tau_{n-2}$ with $n = 2, 3, \ldots, 2N-1$ and $\hat{\tau}_0 = \hat{\tau}_1 = 0$.

By using $2N$ complex-moments $\hat{\tau}_n$ in the annihilating filter method, we design a filter $A[n]$ such that the convolution $\hat{\tau}_n * A[n] = 0$. The N complex roots of the annihilating filter $A(z)$ provide positions (in $x + iy$ form) of the N corner points of the polygon $g(x, y)$. Assumption of convexity and bilevelness[1] guarantees a uniqueness of polygonal reconstruction. Consequently, it follows that

Proposition 3: A bilevel and convex polygon $g(x, y)$ with N corner points is uniquely determined from its samples $S_{j,k} = \langle g(x, y), \varphi_{xy}(x/T_x - j, y/T_y - k)\rangle$ provided that the sampling kernel $\varphi_{xy}(x, y)$ can reproduce polynomials up to degree $2N - 3$ along both the Cartesian axes x and y.

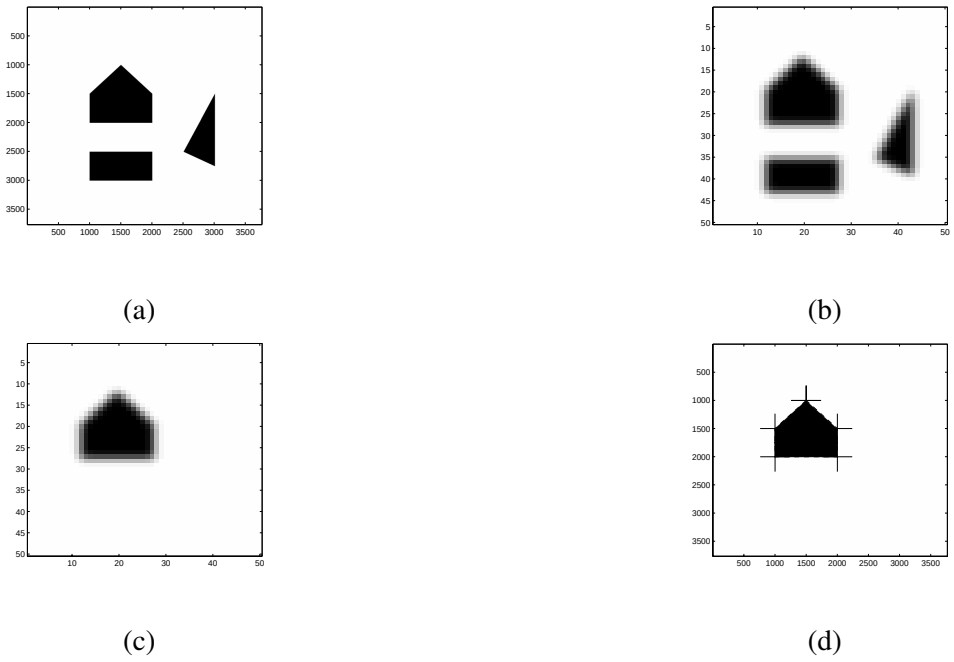

(a) (b) (c) (d)

Fig. 6. Simulation: (a) The original image $g(x, y)$ consists of three bilevel polygons: triangle, rectangle, and pentagon. (b) The set of samples $S_{j,k}$ produced by the inner product between $g(x, y)$ and a B-Spline sampling kernel $\beta^7_{xy}(x, y)$ that can reproduce polynomials up to degree seven. (c) Sampled version of the pentagon. (d) Original pentagon and five reconstructed corner points (marked with $+$).

Simulation result, for a simple scenario, is shown in Figure 6. Figure 6(a) shows a bilevel image $g(x, y)$ that consists of three polygons: triangle, rectangle, and pentagon. Assume that the polygons are enough apart such that in the sampled version of $g(x, y)$ as shown in part (b), they do not overlap. From these samples, by computing sufficient complex-moments $\hat{\tau}_n$, we can retrieve the exact locations of the corner points for each polygonal shape individually. For instance, a set of samples around the pentagon is given in part (c). The reconstructed corner points of the pentagon are indicated with $+$ in part (d) and the reconstruction is exact to machine precision. The

[1]If the convex polygon is large enough such that there is at least one sample enclosed within the polygonal boundary then we can reconstruct its amplitude as well.

computational cost of this global reconstruction is influenced by the cost of root finding and is of the order of $\mathcal{O}(N^3)$ where N is the number of corner points.

C. Diracs, Polygonal Lines, and Quadrature Domains

Together with bilevel polygons there are other 2-D signals that are uniquely determined by a finite number of moments. We now investigate sampling of such signals.

Diracs: Assume $g(x,y)$ is a set of N 2-D Diracs in the closure Ω, that is $g(x,y) = \sum_{l=1}^{N} a_l \delta_{xy}(x - x_l, y - y_l)$, where a_l denotes amplitudes and $z_l = x_l + iy_l$ denotes positions. Clearly, $g(x,y)$ is not regular in Ω, therefore we cannot apply Davis's theorem. However, it is possible to compute the simple complex-moments τ_n of $g(x,y)$ as given by

$$\begin{aligned} \tau_n &= \int\int_{\Omega} g(x,y)\,(x+iy)^n\,dx\,dy \\ &= \int\int_{\Omega} \sum_{l=1}^{N} a_l \delta_{xy}(x - x_l, y - y_l)(x+iy)^n\,dx\,dy \\ &= \sum_{l=1}^{N} a_l\, z_l^n, \quad \text{where } z_l = x_l + iy_l. \end{aligned} \tag{28}$$

The amplitudes a_l and positions z_l of the Diracs are accurately retrieved from $2N$ complex-moments $\tau_n, n = 0, 1, \ldots, 2N-1$ using the annihilating filter method.

Since we have access to $g(x,y)$ in form of its samples $S_{j,k} = \langle g(x,y), \varphi_{xy}(x/T_x - j, y/T_y - k)\rangle$, the moments τ_n of Diracs are obtained from their samples $S_{j,k}$ using (24) and (25), where $\alpha, \beta \in \{0, 1, \ldots, 2N-1\}$. Thus, Proposition 3 can be extend for the set of N 2-D Diracs provided that the kernel $\varphi_{xy}(x,y)$ can reproduce polynomials up to degree $2N-1$ alon both the coordinate axis x and y.

Polygonal lines: Now consider $g(z) = g(x,y)$ to be a set of N unit amplitude polygonal lines representing the boundary $d\Omega$ of the convex polygonal closure Ω. The closed set of polygonal lines $g(z)$ join the corner points $z_l, l = 1, 2, \ldots, N$ in counter-clockwise direction such that $z_l = z_{l+N}$, and is regular over $d\Omega$. Consider an analytic function $h(z)$ in the closure Ω such that Green's theorem with the help of Cauchy-Riemann equations satisfies [25]

$$\int\int_{\Omega} g^*(z) h^{(1)}(z)\,dx\,dy = \frac{i}{2} \int_{d\Omega} g^*(z) h(z)\,dz^*, \quad dz^* = dx - idy, \tag{29}$$

where $g^*(z) = g(z) = 1$ for the set of unit amplitude polygonal lines.

Furthermore, the equation of an arbitrary line PQ joining two points $P(z_1)$ and $Q(z_2)$ in the complex Cartesian

plane $(z = x + iy)$ is given by [25]

$$\begin{aligned} z^* &= \left(\frac{z_1^* - z_2^*}{z_1 - z_2}\right) z + \left(\frac{z_1 z_2^* - z_2 z_1^*}{z_1 - z_2}\right) \\ &= Mz + B, \end{aligned} \tag{30}$$

where z^* is the complex conjugate of z, $M = \frac{z_1^* - z_2^*}{z_1 - z_2}$ is a slope, and $B = \frac{z_1 z_2^* - z_2 z_1^*}{z_1 - z_2}$ is a shift.

From (30), it follows that

$$dz^* = M dz. \tag{31}$$

Now by employing $h(z) = z^n, n \in \mathbb{N}$ in (29) and using (30), (31), we have

$$\begin{aligned} \frac{i}{2}\left[\sum_{l=1}^{N} M_l \int_{z_l}^{z_{l+1}} z^n \, dz\right] &= \frac{i}{2}\int_{d\Omega} g^*(z) h(z) \, dz^* \\ &= \int\int_{\Omega} g(z) \, h^{(1)}(z) \, dx \, dy \\ &= n \int\int_{\Omega} g(x,y) \, (x+iy)^{n-1} \, dx \, dy \\ &= \hat{\tau}_n, \quad n \geq 1, \end{aligned} \tag{32}$$

where $\hat{\tau}_n$ is a complex-moment with weight n, and in this case it is related to τ_n by $\hat{\tau}_n = n\tau_{n-1}$ with $\hat{\tau}_0 = 0$. The coefficient M_l denotes the slope of the polygonal line joining corner points z_l and z_{l+1}.

The left-hand side of (32) reveals that the moments $\hat{\tau}_n$ are in form of linear combinations of the powers of z_l. Therefore, the annihilating filter method can retrieve the N corner points z_l using $2N$ complex moments $\hat{\tau}_n, n = 0, 1, \ldots, 2N-1$. Recall that the moments $\hat{\tau}_n = n\tau_{n-1}$ of $g(x,y)$ are computed from its samples $S_{j,k}$ using (24) and (25) with $\alpha, \beta \in \{0, 1, \ldots, 2N-2\}$. Hence, Proposition 3 can be extend for the convex set of N polygonal lines $g(x,y)$ provided that the kernel $\varphi_{xy}(x,y)$ can reproduce polynomials up to degree $2N-2$ along x and y.

Quadrature domains: Finally, we consider a class of bounded planar domains in the complex plane $z = x + iy$. A quadrature domain Ω is a planar domain that has real algebraic boundary determined by a polynomial equation: $\Omega = \{z \in \mathbb{C}; P(z, z^*) < 0\}$, where $P(z, z^*)$ is a polynomial of degree less than or equal to N in each variable, and N denotes the order of the quadrature domain [18]. The examples of quadrature domains are circles and ellipses (with $N = 1$), and cardioids and lemniscates (with $N = 2$). For a complete treatment on quadrature domains, we refer to [28], [29].

In particular, consider the quadrature domain $g(x,y) \subset \Omega$ whose boundary is expressed by the algebraic equation

$$P(x,y) = P(z, z^*) = 0, \quad \text{with} \quad x = \frac{z + z^*}{2}, \; y = \frac{z - z^*}{2i}. \tag{33}$$

In [18], it was shown that the domain $g(x, y)$ satisfying (33) can be uniquely reconstructed from its finite complex-moments $\tau_{\alpha,\beta}$, $\alpha, \beta \leq N$ as defined in (22), where N is the order of the domain $g(x, y)$. In fact, the reconstruction involves complex mapping (i.e. exponential transformation) of the moments $\tau_{\alpha,\beta}$, $\alpha, \beta \leq N$ to derive an annihilating filter $A[l]$, $l = 0, 1, \ldots, N$ such that its coefficients produce a polynomial

$$p(z) = A[0]z^N + A[1]z^{N-1} + \ldots + A[N]z^0. \tag{34}$$

The polynomial manipulations of $p(z)$ give the expression $P(z, z^*) = 0$ that characterizes a given quadrature domain $g(x, y)$. Moreover, any bounded planar domain can be approximated by a sequence of quadrature domains, and therefore can be approximated by a finite number of moments [18].

Since it is possible to obtain the moments of $g(x, y)$ from its samples $S_{j,k}$, Proposition 3 can be extended for the quadrature domain of order N provided that the kernel can reproduce polynomials up to degree N along x and y directions.

V. Tomographic Approach

Before we present the last approach, we would like to mention that there are many interesting papers in computed tomography (CT) that exploit Radon transform for parametric and nonparametric estimation of multidimensional shapes and contours from noisy tomographic data (e.g. [19], [30], [31]). In particular, the approach of [30] considers estimation of polygonal and polyhedral corner points in Bayesian framework, where as the focus of [31] is on information-theoretic issues in nonparametric boundary estimation.

In this section, we concentrate on sampling and perfect reconstruction of multidimensional FRI signals using the link between Radon transform projections and moments [19]. In particular, we show that, in addition to polygons and Diracs, it is possible to reconstruct more general FRI signals such as 2-D polynomials with polygonal boundaries from their samples. The key feature of the proposed scheme is an annihilating-filter-based-back-projection (AFBP) algorithm.

A. 2-D Polynomials with Polygonal Boundaries

Radon transform: Let $g(x, y)$ be a 2-D square-integrable function within a compact region Ω over the Euclidean space $\mathbb{R}^2$. Then, the conventional Radon transform projection of $g(x, y)$ is defined as [32] (see Figure 7(b)):

$$R_g(t, \theta) = \int\int_{\Omega} g(x, y)\, \delta\left(t - x\cos(\theta) - y\sin(\theta)\right)\, dx\, dy, \tag{35}$$

where the projection angle $\theta \in [0, \pi)$, and $l_{t,\theta} = \delta\left(t - x\cos(\theta) - y\sin(\theta)\right)$ is a straight line of integration at an angle $\theta + \frac{\pi}{2}$ with the x-axis and at a radial distance t away from the origin. The projections $R_g(t, \theta)$ are square integrable 1-D functions with finite support. The original function $g(x, y)$ can again be reconstructed from its projections $R_g(t, \theta)$ using filtered back-projection (FBP) reconstruction [32].

AFBP Algorithm: Consider a specific case, where $g(x, y)$ is a 2-D polynomial of total degree $R - 1$ inside a convex polygonal closure Ω with N corner points. To be more precise, $g(x, y) = \sum_{j=0}^{R-1} \sum_{k=0}^{j} b_{j,k}\, x^k y^{j-k}$ [33], [34]. In this case, we observe that

(a) Each projection $R_g(t, \theta)$ is a 1-D piecewise polynomial of maximum degree R and with at most N discontinuities. Therefore, the $(R+1)$-order derivative of such projection leads to a stream of at most N differentiated Diracs $d_t^{(R+1)}\left[R_g(t, \theta)\right] = \frac{d^{R+1}}{dt^{R+1}}\left[R_g(t, \theta)\right] = \sum_{i=0}^{N-1} \sum_{r=0}^{R} a_{i,r} \delta^{(r)}(t - t_i)$, where t_i are locations and $a_{i,r}$ are weights. It means that $d_t^{(R+1)}\left[R_g(t, \theta)\right]$ represents at most N Diracs with $\hat{N} = N(R+1)$ weights [12], [4]. A simple illustration of this scenario is given in Figure 7.

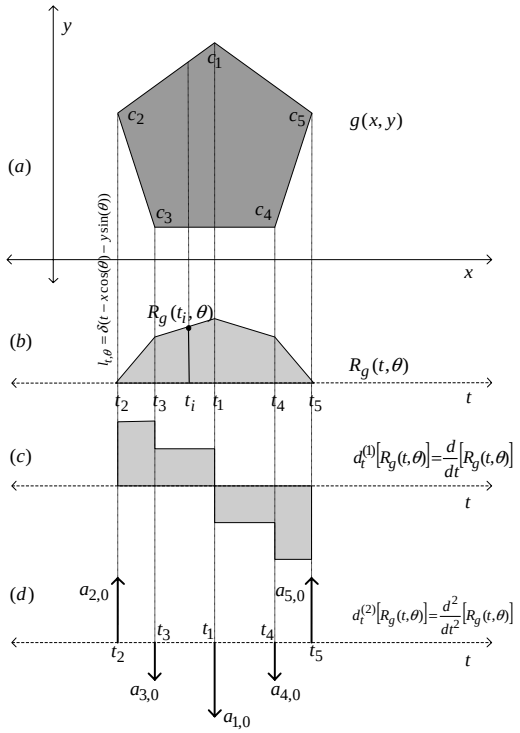

Fig. 7. AFBP reconstruction: The polynomial $g(x, y)$ of degree $R - 1 = 0$ inside a convex polygon with $N = 5$ corner points (i.e. bilevel pentagon) is shown in part (a). The Radon transform projection $R_g(t, \theta)$ along an angle $\theta = 0$ is shown in part (b). Note that $R_g(t_i, \theta)$ is a single-valued line-integral at an arbitrary $t = t_i$ within the support of $R_g(t, \theta)$. Since this projection $R_g(t, \theta)$ is a piecewise polynomial of degree $R = 1$, the $R + 1 = 2$-nd order derivative can decompose it in a stream of differentiated Diracs $d_t^{(2)}\left[R_g(t, \theta)\right]$ as shown in part (d). In this case $d_t^{(2)}\left[R_g(t, \theta)\right]$ represents N Diracs with $\hat{N} = N$ weights.

(b) Moreover, following the connection between Radon projections and moments [19], the moments μ_n, $n \in \mathbb{N}$ of the differentiated Diracs $d_t^{(R+1)}\left[R_g(t,\theta)\right]$ are obtained by

$$\begin{aligned}\mu_n &= \int d_t^{(R+1)}\left[R_g(t,\theta)\right] t^n \, dt \\ &= \int\int_{\Omega} d_\theta^{(R+1)}\left[g(x,y)\right] \left(x\cos(\theta)+y\sin(\theta)\right)^n \, dx\, dy \\ &= \sum_{\beta=0}^{n} \binom{n}{\beta} \cos^{\alpha}(\theta)\sin^{\beta}(\theta)\, \mu_{\alpha,\beta}, \quad \text{with} \quad \alpha = n-\beta, \end{aligned} \tag{36}$$

where $\mu_{\alpha,\beta} = \int\int_{\Omega} \frac{d^{R+1}}{d\theta^{R+1}}\left[g(x,y)\right] x^{\alpha}y^{\beta} \, dxdy$ are the geometric moments of the polynomial $g(x,y)$ differentiated $R+1$ times along the direction of θ.

(c) Since the projection $d_t^{(R+1)}\left[R_g(t,\theta)\right]$ consists of at most N Diracs with $\hat{N} = N(R+1)$ weights, the $2\hat{N} = 2N(R+1)$ moments $\mu_n, n = 0, 1, \ldots, 2N(R+1)-1$ are sufficient to retrieve the locations t_i and weights $a_{i,r}$ of the Diracs $d_t^{(R+1)}\left[R_g(t,\theta)\right]$ (and therefore the piecewise polynomial signal $R_g(t,\theta)$ itself) using annihilating filter method [12], [4].

(d) By iterating the steps (a), (b), and (c) over $N+1$ distinct projection angles $\theta_l, l = 0, 1, \ldots, N$, it is possible to retrieve the $N+1$ sets of Dirac locations t_i. By back-projecting the $N+1$ sets of Dirac locations t_i, the N corner points of the convex closure Ω are uniquely determined, and therefore, the closure of $g(x,y)$ itself [11], [35].

(e) From the knowledge of closure Ω and Radon projection $R_g(t,\theta)$, we have access to the single-valued line-integral $R_g(t_i,\theta)$ for an arbitrary $t = t_i$ within the support of $R_g(t,\theta)$ (see Figure 7(b)). In fact, $R_g(t_i,\theta) = \int_{l_{t_i,\theta}} g(x,y)\, dl = \int_{l_{t_i,\theta}} \left(\sum_{j=0}^{R-1}\sum_{k=0}^{j} b_{j,k}\, x^k y^{j-k}\right) dl$ is an equation with $\hat{R} = R(R+1)/2$ unknown coefficients $b_{j,k}$. Clearly, the coefficients $b_{j,k}$ can be determined by solving a system of $\hat{R}$ such equations (i.e. a generalized Vandemonde system). Fortunately, the theory of bivariate polynomial interpolation [33], [34] assures a unique solution if at least R distinct projections $R_g(t,\theta)$ are known.[2] Since $N+1$ projections are required for recovering the closure Ω, and R projections are required for determining the coefficients $b_{j,k}$, we are sure that $\max(N+1, R)$ projections are sufficient for the unique reconstruction of $g(x,y)$.

To summarize, if $g(x,y)$ is a 2-D polynomial of degree $R-1$ inside a convex polygonal closure Ω with N corner points, then from the moments μ_n we can retrieve the projection $R_g(t,\theta)$ and from $\max(N+1, R)$ such projections

[2] In fact, R projections $R_g(t,\theta)$ are exploited to obtain $\hat{R} = R(R+1)/2$ line-integrals $R_g(t_i,\theta)$ using arithmetic progression [33]. It is straightforward to obtain a unique (but suboptimal) solution by directly using $\hat{R}$ distinct projections $R_g(t,\theta)$ [36].

we can retrieve the polygonal closure Ω first and the coefficients $b_{j,k}$ next. Notice that the crucial part of above reconstruction is the recovery of corner points. Since the retrieval of corner points is based on annihilating filter, we denote the proposed reconstruction as: annihilating filter based back projection (AFBP) algorithm. Equipped with the Radon-moment connection (36) and AFBP algorithm, we now show that the 2-D polynomials with polygonal boundaries can be uniquely reconstructed from their samples. Similar results can be obtained for other 2-D FRI signals such as sets of 2-D Diracs, and bilevel-convex polygons.

Sampling: Assume that $g(x,y) = \sum_{j=0}^{R-1} \sum_{k=0}^{j} b_{j,k}\, x^k y^{j-k}$ is a 2-D polynomial of degree $R-1$ with at most $\hat{R}$ coefficients $b_{j,k}$ inside the convex polygonal closure Ω with N corner points. We observe the samples $S_{j,k}$ of $g(x,y)$ given by $S_{j,k} = \langle g(x,y), \varphi_{xy}(x/T_x - j, y/T_y - k)\rangle$, where $\varphi_{xy}(x,y)$ is the sampling kernel that can reproduce polynomials up to degree n along x and y directions.

Recall that in order to retrieve the corner points of the closure Ω, we need to compute the moments μ_n of the differentiated projections $d_t^{(R+1)}\left[R_g(t,\theta)\right]$ from the moments $\mu_{\alpha,\beta}$ of the differentiated polynomial $d_\theta^{(R+1)}\left[g(x,y)\right]$ as given in (36). Nevertheless, from lattice theory, it is possible to show that there exists a direction vector $\vec{v} = [v_x, v_y]$ along a chosen projection angle $\theta = \tan^{-1}(\frac{v_y}{v_x})$, $v_x, v_y \in \mathbb{Z}$ such that the discrete domain directional differences $\mathcal{D}_\theta^{(R+1)}\left[S_{j,k}\right]$ and the continuous domain directional derivatives $d_\theta^{(R+1)}\left[g(x,y)\right]$ are related by (see Appendix-I):

$$R_{j,k} = \mathcal{D}_\theta^{(R+1)}\left[S_{j,k}\right] = \left\langle d_\theta^{(R+1)}\left[g(x,y)\right], \zeta_\theta(x/T_x - j, y/T_y - k)\right\rangle. \tag{37}$$

The new set of samples $R_{j,k} = \mathcal{D}_\theta^{(R+1)}\left[S_{j,k}\right]$, obtained by the $(R+1)$-order directional differences on the set of samples $S_{j,k}$, is equivalent to one produced by the inner products between the differentiated polynomial $d_\theta^{(R+1)}\left[g(x,y)\right]$ and the modified (directional) kernel $\zeta_\theta(x,y)$. The kernel $\zeta_\theta(x,y)$ is produced by $R+1$ successive convolutions of zero-th order 1-D B-spline $\beta_\theta^0(x,y)$ with the original sampling kernel $\varphi_{xy}(x,y)$ in the direction of $\vec{v}$. More precisely, $\zeta_\theta(x,y) = |v|^{(R+1)}\ \left(\varphi_{xy}(x,y) * \beta_\theta^R(x,y)\right)$.

It is important to note that the directional kernel also satisfies the polynomial reproduction property of (5). In particular, if the sampling kernel $\varphi_{xy}(x,y)$ can reproduce polynomials up to degree n along x and y, then the directional kernel $\zeta_\theta(x,y)$ can reproduce polynomials up to degree $n+R+1$ along θ.

In the light of link (37), equations (36) and (25) enable us to obtain the moments μ_n of the projection $d_t^{(R+1)}\left[R_g(t,\theta)\right]$ using linear combinations of samples $R_{j,k}$ and coefficients $C_{j,k}^{\alpha,\beta}$ as given by

$$\mu_n = \sum_{\beta=0}^{n} \binom{n}{\beta} \cos^\alpha(\theta)\, \sin^\beta(\theta) \left(\sum_j \sum_k R_{j,k}\, C_{j,k}^{\alpha,\beta}\right), \quad \text{with} \quad \alpha = n-\beta, \tag{38}$$

where $C_{j,k}^{\alpha,\beta}$ are the coefficients associated with the kernel $\zeta_\theta(x,y)$.

Since $d_t^{(R+1)}\left[R_g(t,\theta)\right]$ consists of at most N Diracs with $\hat{N} = N(R+1)$ weights, the directional kernel $\zeta_\theta(x,y)$ must allow us to retrieve $2\hat{N} = 2N(R+1)$ moments $\mu_n, n = 0,1,\ldots,2N(R+1)-1$, and thus it follows that

$$n + R + 1 \geq 2N(R+1) - 1 \quad \Rightarrow \quad n \geq (2N-1)(R+1) - 1. \tag{39}$$

Therefore, a sampling kernel $\varphi_{xy}(x,y)$ that reproduces polynomial of degree n (with n satisfying (39)) allows us to obtain the $2N(R+1)$ moments of each of $\max(N+1,R)$ differentiated projections $d_t^{(R+1)}\left[R_g(t,\theta_l)\right], l = 0,1,\ldots,\max(N+1,R)-1$ from the samples $R_{j,k} = \mathcal{D}_{\theta_l}^{(R+1)}\left[S_{j,k}\right]$ using (38). Then following the steps (c) and (d) of the AFBP algorithm, we retrieve the convex polygonal closure Ω of $g(x,y)$. Finally, from step (e), we determine the coefficients $b_{j,k}$ of the polynomial of degree $R-1$ inside Ω, and thus the 2-D polynomial signal $g(x,y)$ itself. In summary, we have:

Proposition 4: Assume that $g(x,y)$ is a 2-D polynomial of total degree $R-1$ inside a convex polygonal closure Ω with N corner points. A set of samples $S_{j,k} = \langle g(x,y), \varphi_{xy}(x/T_x - j, y/T_y - k)\rangle$ is sufficient to determine $g(x,y)$ exactly, if the sampling kernel $\varphi_{xy}(x,y)$ can reproduce polynomials at least up to degree $(2N-1)(R+1)-1$ along both the coordinate axes x and y.

For the sake of completeness, we now show with a pseudo-algorithm how the reconstruction scheme operates. Given a valid set of samples $S_{j,k} = \langle g(x,y), \varphi_{xy}(x/T_x - j, y/T_y - k)\rangle$, the reconstruction of 2-D polynomial $g(x,y) = \sum_{j=0}^{R-1}\sum_{k=0}^{j} b_{j,k}\, x^k y^{j-k}$ of degree $R-1$ inside the convex polygonal closure Ω with N corner points follows the following steps:

Algorithm: AFBP reconstruction of 2-D polynomial signal from its samples

1) For a chosen angle $\theta = \tan^{-1}(\frac{v_y}{v_x})$, $v_x, v_y \in \mathbb{Z}$, compute the difference $R_{j,k} = \mathcal{D}_\theta^{(R+1)}\left[S_{j,k}\right]$ given by (37).
2) Using (38), compute the first $2N(R+1)$ moments $\mu_n, n = 0,1,\ldots,2N(R+1)-1$ of the projection $d_t^{(R+1)}\left[R_g(t,\theta)\right]$ from the new set of samples $R_{j,k}$ [recall step (b) of the AFBP algorithm].
3) From moments μ_n, using annihilating filter method, obtain the exact locations $t_i, i = 1,2,\ldots,N$ of the N Diracs of $d_t^{(R+1)}\left[R_g(t,\theta)\right]$, and thus, the projection $R_g(t,\theta)$ itself [step (c)].
4) Iterate steps 1, 2, and 3 for $N+1$ distinct projection angles $\theta_l, l = 0,1,\ldots,N$, and then by back-projecting $N+1$ sets of dirac locations t_i, retrieve the convex polygonal closure Ω of $g(x,y)$ [step (d)].
5) From the knowledge of the closure Ω and Radon projections $R_g(t,\theta_l), l = 0,1,\ldots,R-1$, determine the coefficients $b_{j,k}$ of the polynomial $g(x,y)$ by solving a system of $\hat{R}$ linear equations [step (e)].

6) Since the closure Ω and the coefficients $b_{j,k}$ are known, it is easy to reconstruct the 2-D polynomial $g(x, y)$.

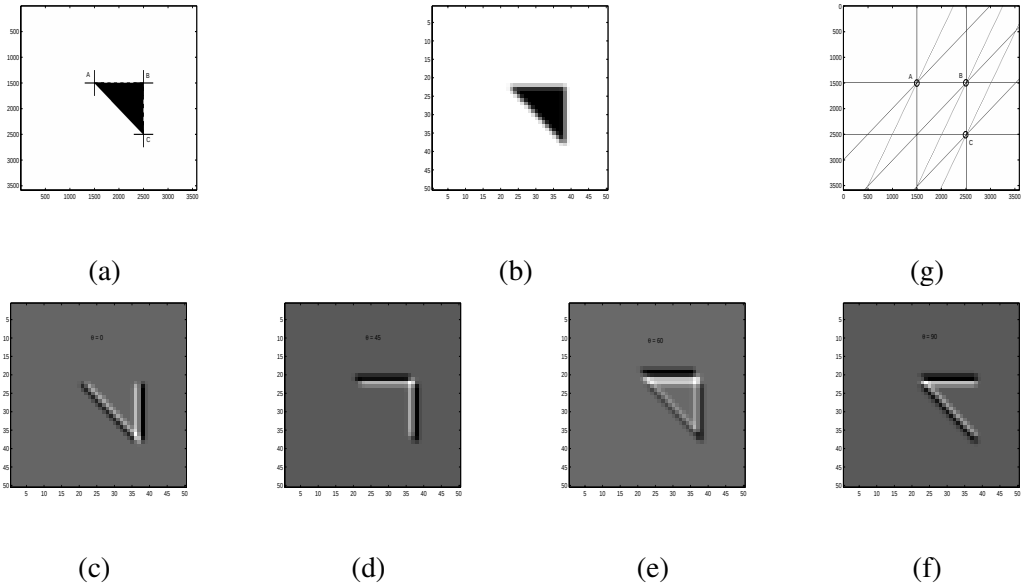

Fig. 8. Simulation: The original planar triangle $g(x, y)$, and the reconstructed corner points A, B, and C (marked with +) are given in part (a). The set of samples $S_{j,k}$ produced by the B-spline sampling kernel β^9_{xy} is given in part (b). The $N + 1 = 4$ sets of differentiate samples $R_{j,k} = D^{(2)}_\theta[S_{j,k}]$ along four angles $\theta = 0, \frac{\pi}{4}, \tan^{-1}(2)$, and $\frac{\pi}{2}$ are given in parts (c), (d), (e), and (f). The AFBP reconstruction of the corner points A, B, and C is illustrated in part (g).

A simple simulation result is shown in Figure 8. In this case, $g(x, y)$ is a 2-D polynomial of degree $R - 1 = 0$ (i.e $g(x, y) = b_{0,0}$) inside a convex polygonal closure Ω with $N = 3$ corner points. In part (a), the original polynomial $g(x, y)$ is shown with the reconstructed corner points (marked with $+$). The samples $S_{j,k} = \langle g(x, y), \varphi_{xy}(x/T_x - j, y/T_y - k)\rangle$ are shown in part (b), where $\varphi_{xy}(x, y)$ is a B-spline sampling kernel that can reproduce polynomials up to degree $n = (2N - 1)(R + 1) - 1 = 9$ along x and y directions, and therefore, the associated directional kernels $\zeta_{\theta_l}(x, y)$ can reproduce polynomials up to degree $n + R + 1 = 11$ along θ_l. The sets of differentiated samples $R_{j,k} = D^2_{\theta_l}[S_{j,k}]$ along four distinct angles $\theta_0 = 0, \theta_1 = \frac{\pi}{4}, \theta_2 = \tan^{-1}(2)$ and $\theta_3 = \frac{\pi}{2}$ are shown in parts (c), (d), (e), and (f). The AFBP reconstruction of the corner points (marked with $\circ$) using $N+1 = 4$ back-projections is shown in part (g), and is exact to machine precision. These corner points can uniquely recover the convex closure Ω. Form the knowledge of Ω and any one projection $R_g(t, \theta_l)$, we can uniquely retrieve the coefficient $b_{0,0}$, and thus the polynomial $g(x, y)$ itself.

In this case, the benefit of reconstructing more general signals comes with the price of higher computational cost. For instance, for a 2-D polynomial of degree $R - 1 = 0$ inside a convex polygon with N corner points, the computational cost is of the order of $\mathcal{O}(N^4)$. This is due to the fact that the cost of finding the roots of each Radon projection is $\mathcal{O}(N^3)$ and we need $\mathcal{O}(N)$ projections to reconstruct the polynomial.

VI. CONCLUSION

In this paper, we have presented various schemes for sampling and perfect reconstruction of multidimensional FRI signals using kernels that reproduce polynomials. In particular, we offer local and global reconstruction methods with varying complexities as summarized in Table I. The issues of model mismatch and noise effects are beyond the scope of this paper but are still open for further investigation.

TABLE I

COMPARATIVE SUMMARY

Approach	**Signals**	**Merits**	**Computational cost**	**Limitations**
Directional derivatives (Local)	Planar polygons.	Local reconstruction, local complexity.	$\mathcal{O}(N)$ for polygon with N corner points.	Finite orientations of polygonal sides, i.e. $\tan(\theta) \in \mathbb{Q}$.
Complex-moments (Global)	Convex and bilevel polygons, Quadrature domains (e.g. ellipses, cardioids), Polygonal lines, and 2-D Diracs.	Reconstruction of corner points with any coordinates.	$\mathcal{O}(N^3)$ for bilevel-convex polygon with N corner points.	Numerically unstable for closely spaced corner points.
Tomographic (Global)	2-D polynomials with polygonal boundaries, n-D Diracs, and n-D bilevel-convex polytopes.	Multidimensional.	$\mathcal{O}(N^4)$ for 2-D polynomial of degree $R-1=0$ inside convex polygon with N corner points.	Numerical instability in computation of higher order moments with directional kernels.

In Section III, we described a directional derivatives based local approach for reconstruction of planar polygons from their samples using lower order kernels that satisfy partition of unity. This scheme has a local complexity irrespective of the number of corner points in a given polygon. In Section IV, we presented a complex-moments based global reconstruction scheme for convex and bilevel polygons, and extended it for quadrature domains that are capable of approximating arbitrary planar shapes with closed boundaries. Finally, we presented a Radon transform based scheme for sampling more general FRI signals such as 2-D polynomials with polygonal boundaries in Section V. Since the Radon transform is multidimensional, it is straightforward to extend the AFBP algorithm for

sampling bilevel-convex polytopes and Diracs in higher dimensions (i.e. in 3-D and above).

The proposed schemes may find their applications in vectored graphics, computer animations, and machine vision. In fact, the proposed schemes have been promisingly explored for super-resolution algorithms [5] and distributed compression [6]. Finally, the use of the corner reconstruction algorithm for super-resolution photogrammetry is under investigation.

ACKNOWLEDGMENT

Authors are thankful to Prof. Martin Vetterli and Dr. Thierry Blu for their suggestions.

APPENDIX I

CONNECTION BETWEEN DIRECTIONAL DIFFERENCES AND DERIVATIVES: EQUATION (18)

Consider the set of samples $S_{j,k} = \langle g(x,y), \varphi_{xy}(x/T_x - j, y/T_y - k\rangle$ of a planar polygon $g(x,y)$, where $\varphi_{xy}(x,y)$ is the sampling kernel, and let the sampling intervals $T_x = T_y = 1$. Now apply a pair of finite differences $\mathcal{D}^{(1)}_{\theta_1}[\cdot]$ and $\mathcal{D}^{(1)}_{\theta_2}[\cdot]$ on samples $S_{j,k}$, first along the lattice direction $\vec{v}_1$ and then along $\vec{v}_2$ to obtain the new set of samples $R_{j,k}$ given by

$$\begin{aligned} R_{j,k} &= \mathcal{D}^{(1)}_{\theta_2}\Big[\mathcal{D}^{(1)}_{\theta_1}[S_{j,k}]\Big] = \big\{S_{(j+v_{2,1}+v_{1,1}),(k+v_{2,2}+v_{1,2})} - S_{(j+v_{2,1}),(k+v_{2,2})}\big\} - \big\{S_{(j+v_{1,1}),(k+v_{1,2})} - S_{j,k}\big\} \\ &= \Big\langle g(x,y), \Big\{\varphi_{xy}\big(x-(j+v_{2,1}+v_{1,1}), y-(k+v_{2,2}+v_{1,2})\big) - \varphi_{xy}\big(x-(j+v_{2,1}), y-(k+v_{2,2})\big)\Big\} - \\ &\quad \Big\{\varphi_{xy}\big(x-(j+v_{1,1}), y-(k+v_{1,2})\big) - \varphi_{xy}\big(x-j, y-k\big)\Big\}\Big\rangle. \end{aligned}$$

Using Parseval's identity, it follows that

$$\begin{aligned} R_{j,k} &= \frac{1}{4\pi^2}\Big\langle \hat{g}(\omega_x,\omega_y), \hat{\varphi}_{xy}(\omega_x,\omega_y)\cdot e^{-i(j\omega_x+k\omega_y)}\cdot\Big(\Big\{e^{-i\left((v_{2,1}+v_{1,1})\omega_x+(v_{2,2}+v_{1,2})\omega_y\right)} - e^{-i\left(v_{2,1}\omega_x+v_{2,2}\omega_y\right)}\Big\} - \\ &\quad \Big\{e^{-i\left(v_{1,1}\omega_x+v_{1,2}\omega_y\right)} - 1\Big\}\Big)\Big\rangle \\ &= \frac{1}{4\pi^2}\Big\langle \hat{g}(\omega_x,\omega_y), \hat{\varphi}_{xy}(\omega_x,\omega_y)\cdot e^{-i(j\omega_x+k\omega_y)}\cdot\Big(e^{-i\left(v_{1,1}\omega_x+v_{1,2}\omega_y\right)} - 1\Big)\cdot\Big(e^{-i\left(v_{2,1}\omega_x+v_{2,2}\omega_y\right)} - 1\Big)\Big\rangle, \end{aligned}$$

where $i = \sqrt{-1}$, and $\hat{g}(\omega_x,\omega_y)$ and $\hat{\varphi}_{xy}(\omega_x,\omega_y)$ are the 2-D Fourier transforms of $g(x,y)$ and $\varphi_{xy}(x,y)$ respectively. After multiplying and dividing by the same factors, we have that

$$\begin{aligned} R_{j,k} &= \frac{1}{4\pi^2}\Bigg\langle \hat{g}(\omega_x,\omega_y), \hat{\varphi}_{xy}(\omega_x,\omega_y)\cdot e^{-i(j\omega_x+k\omega_y)}\cdot\Big(i\big(v_{1,1}\omega_x+v_{1,2}\omega_y\big)\Big)\cdot\Big(i\big(v_{2,1}\omega_x+v_{2,2}\omega_y\big)\Big)\cdot \\ &\quad \frac{\Big(e^{-i\left(v_{1,1}\omega_x+v_{1,2}\omega_y\right)} - 1\Big)\Big(e^{-i\left(v_{2,1}\omega_x+v_{2,2}\omega_y\right)} - 1\Big)}{\Big(i\big(v_{1,1}\omega_x+v_{1,2}\omega_y\big)\Big)\Big(i\big(v_{2,1}\omega_x+v_{2,2}\omega_y\big)\Big)}\Bigg\rangle. \end{aligned} \tag{40}$$

Now recall that $\hat{\beta}^0(\omega) = \frac{1-e^{-i\omega t}}{i\omega}$ is a frequency domain representation of the zero-th order 1-D B-spline $\beta^0(t)$. This representation can be extended for 1-D directional B-spline in 2-D plane as given by

$$\hat{\beta}^0_{\theta_1}(\omega_x,\omega_y) = \frac{\big(1-e^{-i(v_{1,1}\omega_x+v_{1,2}\omega_y)}\big)}{i(v_{1,1}\omega_x+v_{1,2}\omega_y)}, \quad \hat{\beta}^0_{\theta_2}(\omega_x,\omega_y) = \frac{\big(1-e^{-i(v_{2,1}\omega_x+v_{2,2}\omega_y)}\big)}{i(v_{2,1}\omega_x+v_{2,2}\omega_y)}, \tag{41}$$

where $\hat{\beta}^0_{\theta_1}$ and $\hat{\beta}^0_{\theta_2}$ are the 1-D B-splines of order zero in 2-D plane along orientations $\theta_1 = \tan^{-1}\left(\frac{v_{1,2}}{v_{1,1}}\right)$ and $\theta_2 = \tan^{-1}\left(\frac{v_{2,2}}{v_{2,1}}\right)$ respectively. For simplicity, let

$$\hat{\xi}_{\theta_1,\theta_2}(\omega_x,\omega_y) = \hat{\varphi}_{xy}(\omega_x,\omega_y)\,\hat{\beta}^0_{\theta_1}(\omega_x,\omega_y)\,\hat{\beta}^0_{\theta_2}(\omega_x,\omega_y). \tag{42}$$

Replacing (41) and (42) in the formulation of (40), and then multiplying and dividing by a factor $|v_1||v_2|$, we have

$$\begin{aligned} R_{j,k} &= \frac{|v_1||v_2|}{4\pi^2}\Bigg\langle \hat{g}(\omega_x,\omega_y), \hat{\xi}_{\theta_1,\theta_2}(\omega_x,\omega_y)\cdot e^{-i(j\omega_x+k\omega_y)}\,\cdot \\ &\quad \Big\{(i\omega_x)^2\frac{v_{1,1}\,v_{2,1}}{|v_1||v_2|} + (i\omega_x)(i\omega_y)\frac{(v_{1,1}\,v_{2,2}+v_{1,2}\,v_{2,1})}{|v_1||v_2|} + (i\omega_y)^2\frac{v_{1,2}\,v_{2,2}}{|v_1||v_2|}\Big\}\Bigg\rangle. \end{aligned}$$

Using the identities $v_{1,1} = |v_1|\cos(\theta_1),\ v_{1,2} = |v_1|\sin(\theta_1),\ v_{2,1} = |v_2|\cos(\theta_2),\ v_{2,2} = |v_2|\sin(\theta_2)$, $|\det(V_\Lambda)| = |v_{1,1}\,v_{2,2} - v_{1,2}\,v_{2,1}|$, and $|v_1||v_2| = \frac{|\det(V_\Lambda)|}{|\sin(\theta_2-\theta_1)|}$ in the righthand side of the above equation, we have

$$\begin{aligned} R_{j,k} &= \frac{|\det(V_\Lambda)|}{4\pi^2|\sin(\theta_2-\theta_1)|}\Bigg\langle \hat{g}(\omega_x,\omega_y), \hat{\xi}_{\theta_1,\theta_2}(\omega_x,\omega_y)\cdot e^{-i(j\omega_x+k\omega_y)}\,\cdot \\ &\quad \Big\{(i\omega_x)^2\cos(\theta_1)\cos(\theta_2) + (i\omega_x)(j\omega_y)\sin(\theta_1+\theta_2) + (i\omega_y)^2\sin(\theta_1)\sin(\theta_2)\Big\}\Bigg\rangle. \end{aligned}$$

Using Parseval's identity, we have

$$\begin{aligned} R_{j,k} &= \frac{|\det(V_\Lambda)|}{|\sin(\theta_2-\theta_1)|}\Bigg\langle g(x,y), \Big\{\cos(\theta_1)\cos(\theta_2)\frac{\partial^2}{\partial x^2}\Big(\xi_{\theta_1,\theta_2}(x-j,y-k)\Big) + \\ &\quad \sin(\theta_1+\theta_2)\frac{\partial}{\partial y}\Big(\frac{\partial}{\partial x}\Big(\xi_{\theta_1,\theta_2}(x-j,y-k)\Big)\Big) + \sin(\theta_1)\sin(\theta_2)\frac{\partial^2}{\partial y^2}\Big(\xi_{\theta_1,\theta_2}(x-j,y-k)\Big)\Big\}\Bigg\rangle. \end{aligned}$$

Comparing the righthand side of the above equation with the continuous directional derivative model given in equation (17), it follows that

$$\begin{aligned} \frac{R_{j,k}}{|\det(V_\Lambda)|} &= \frac{1}{|\sin(\theta_2-\theta_1)|}\Bigg\langle g(x,y), \frac{\partial}{\partial\theta_2}\Big(\frac{\partial}{\partial\theta_1}\Big(\xi_{\theta_1,\theta_2}(x-j,y-k)\Big)\Big)\Bigg\rangle \\ &\overset{(a)}{=} \Bigg\langle \frac{\partial}{\partial\theta_2}\Big(\frac{\partial}{\partial\theta_1}\Big(g(x,y)\Big)\Big), \frac{1}{|\sin(\theta_2-\theta_1)|}\xi_{\theta_1,\theta_2}(x-j,y-k)\Bigg\rangle \\ &= \Bigg\langle \frac{\partial}{\partial\theta_2}\Big(\frac{\partial}{\partial\theta_1}\Big(g(x,y)\Big)\Big), \zeta_{\theta_1,\theta_2}(x-j,y-k)\Bigg\rangle, \end{aligned} \tag{43}$$

where equality (a) is obtained using integration by parts, and $\zeta_{\theta_1,\theta_2}(x,y) = \frac{\xi_{\theta_1,\theta_2}(x,y)}{|\sin(\theta_2-\theta_1)|} = \frac{\big(\varphi_{xy}(x,y)*\beta^0_{\theta_1}(x,y)\big)*\beta^0_{\theta_2}(x,y)}{|\sin(\theta_2-\theta_1)|}$ is the modified directional kernel.

REFERENCES

[1] P. Shukla and P. L. Dragotti, "Sampling schemes for 2-D signals with finite rate of innovation using kernels that reproduce polynomials," in *Proceedings of IEEE International Conference on Image Processing (ICIP)*, Genova, Italy, September 2005.

[2] ——, "Tomographic approach for sampling multidimensional signals with finite rate of innovation," in *Proceedings of IEEE International Conference on Image Processing (ICIP)*, Atlanta, USA, October 2006.

[3] M. Vetterli, P. Marziliano, and T. Blu, "Sampling signals with finite rate of innovation," *IEEE Transactions on Signal Processing*, vol. 50, no. 6, pp. 1417–1428, June 2002.

[4] P. L. Dragotti, M. Vetterli, and T. Blu, "Sampling moments and reconstructing signals with finite rate of innovation: Shannon meets Strang-Fix," *IEEE Transactions on Signal Processing*, July 2006, accepted.

[5] L. Baboulaz and P. L. Dragotti, "Distributed acquisition and image super-resolution based on continuous moments from samples," in *Proceedings of IEEE International Conference on Image Processing (ICIP)*, Atlanta, GA, USA, October 2006.

[6] N. Gehrig and P. L. Dragotti, "Distributed sampling and compression of scenes with finite rate of innovation in camera sensor networks," in *Proceedings of Data Communication Conference (DCC)*, Snowbird,Utah,USA, March 2006.

[7] A. J. Jerry, "The Shannon sampling theorem—its various extensions and applications: A tutorial review," *Proceedings of the IEEE*, vol. 65, no. 11, pp. 1565–1596, November 1977.

[8] M. Unser, "Sampling—50 Years after Shannon," *Proceedings of the IEEE*, vol. 88, no. 4, pp. 569–587, April 2000.

[9] M. Unser and A. Aldroubi, "A general sampling theory for nonideal acquisition devices," *IEEE Transactions on Signal Processing*, vol. 42, no. 11, pp. 2915–2925, November 1994.

[10] I. Maravić and M. Vetterli, "Exact sampling results for some classes of parametric nonbandlimited 2-D signals," *IEEE Transactions on Signal Processing*, vol. 52, no. 1, pp. 175–189, January 2004.

[11] ——, "A sampling theorem for the Radon transform of finite complexity objects," *Proceedings of IEEE International Conference on Acoustics, Speech and Signal Processing (ICASSP)*, pp. 1197–1200, May 2002.

[12] P. L. Dragotti, M. Vetterli, and T. Blu, "Exact sampling results for signals with finite rate of innovation using Strang-Fix conditions and local kernels," in *Proceedings of IEEE International Conference on Acoustics, Speech and Signal Processing (ICASSP)*, Philadelphia, USA, March 2005.

[13] M. Unser, "Splines - a perfect fit for signal and image processing," *IEEE Signal Processing Magazine*, vol. 16, pp. 22–38, November 1999.

[14] G. Strang and Fix. G., "Fourier analysis of the finite element variational method," *Constructive Aspects of Functional Analysis, Rome, Italy*, pp. 796–830, 1971.

[15] V. Velisavljevic, B. Beferull-Lozano, M. Vetterli, and P. L. Dragotti, "Directionlets: Anisotropic multi-directional representation with separable filtering," *IEEE Transactions on Image Processing*, vol. 15, no. 7, pp. 1916–1933, July 2006.

[16] J. Konrad and P. Agniel, "Subsampling models and anti-alias filters for 3-D automultiscopic displays," *IEEE Transactions on Image Processing*, vol. 15, no. 1, pp. 128–140, January 2006.

[17] J. H. Conway and N. J. A. Sloane, *Sphere Packing, Lattices and Groups*. Springer-Verlag, 1998.

[18] P. Milanfar, M. Putinar, J. Varah, B. Gustafsson, and G. Golub, "Shape reconstruction from moments: theory, algorithms, and applications," *Proceedings of SPIE*, vol. 4116, pp. 406–416, November 2000.

[19] P. Milanfar, G. Verghese, W. Karl, and A. Willsky, "Reconstructing polygons from moments with connections to array processing," *IEEE Transactions on Signal Processing*, vol. 43, no. 2, pp. 432–443, February 1995.

[20] M. Elad, P. Milanfar, and G. H. Golub, "Shape from moments- an estimation theory perspective," *IEEE Transactions on Signal Processing*, vol. 52, no. 7, pp. 1814–1829, July 2004.

[21] I. Daubechies, *Ten Lectures on Wavelets*. Philadelphia, PA: Society for Industrial and Applied Mathematics, 1992.

[22] P. Stoica and R. Moses, *Introduction to Spectral Analysis*. Englewood Cliffs,NJ: Prentice-Hall, 2000.

[23] R. E. Blahut, *Theory and practice of Error Control Codes*. Addison-Wesley, 1983.

[24] M. K. Hu, "Visual pattern reconition by moment invariants," *IRE Transactions on Information Theory*, vol. 8, pp. 179–187, 1962.

[25] P. J. Davis, "Triangle formulas in the complex plane," *Mathematics of Computation*, vol. 18, pp. 569–577, 1964.

[26] C. Teh and R. T. Chin, "On image analysis by the methods of moments," *IEEE Transactions on Pattern Analysis and Machine Intelligence*, vol. 10, no. 4, pp. 496–513, July 1988.

[27] Y. S. Abu-Mostafa and D. Psaltis, "Recognitive aspects of moment invariants," *IEEE Transactions on Pattern Analysis and Machine Intelligence*, vol. 6, pp. 698–706, November 1984.

[28] B. Gustafsson, C. He, P. Milanfar, and M. Putinar, "Reconstructing planar domains from their moments," *Inverse Problems*, vol. 16, no. 4, pp. 1053–1070, August 2000.

[29] H. S. Shapiro, *The Schwartz function and its generalization to higher dimensions*. Wiley, New York, 1992.

[30] C. Soussen and A. Mohammad-Djafari, "Polygonal and polyhedral contour reconstruction in computed tomography," *IEEE Transactions on Image Processing*, vol. 13, no. 11, pp. 1507–1523, November 2004.

[31] A. Goldenshluger and V. Spokoiny, "Recovering convex edges of an image from noisy tomographic data," *IEEE Transactions on Information Theory*, vol. 52, no. 4, pp. 1322–1334, April 2006.

[32] S. R. Deans, *The Radon Transform and Some of Its Applications*. John Wiley, 1983.

[33] B. Bojanov and I. K. Georgieva, "Interpolation by bivariate polynomials based on Radon projections," *Studia Math.*, vol. 162, no. 2, pp. 141–160, 2004.

[34] B. Bojanov and Y. Xu, "Reconstruction of a polynomial from its Radon projections," *SIAM J. Math. Anal.*, vol. 37, no. 1, pp. 238–250, September 2005.

[35] Y. Bresler, "Model based estimation techniques for 3-D reconstruction from projections," Ph.D. dissertation, Stanford University, Stanford, CA, USA, 1985.

[36] H. Hakopian, "Multivariate divided differences and multivariate interpolation of Lagrange and Hermite type," *J. Approx. Theory*, vol. 34, pp. 286–305, 1982.

PLACE PHOTO HERE

Pancham Shukla (S'05) is currently writing up his Ph.D. thesis at Imperial College London. He received his Master of Philosophy (M.Phil.) degree in Electrical and Electronic Engineering from the University of Strathclyde, Glasgow, UK in 2003, and the Master (M.E.) and the Bachelor (B.E.) degrees in Electronic Engineering from BVM Engineering College, Sardar Patel University, Gujarat, India in 2001 and 1995 respectively.

Since November 2003, he is a Research Staff at Imperial College London. From October 2002 to October 2003 he was a Teaching and Research Assistant at the University of Strathclyde, Glasgow, UK. From 1996 to 2002, he was a Lecturer at Sardar Patel University, Gujarat, India. He was a visiting researcher at Space Application Center (SAC-ISRO), Ahmedabad, India in 2000.

His current research is focused toward wavelets, approximation theory, and multidimensional sampling. He is interested in mathematical as well as applied signal processing.

PLACE PHOTO HERE

Pier Luigi Dragotti (M'02) received the Laurea Degree (summa cum laude) in Electrical Engineering from the University Federico II, Naples, Italy, and the Master degree in Communications Systems and the Ph.D degree from the Swiss Federal Institute of Technology, Lausanne (EPFL), Switzerland in 1997, 1998, and 2002, respectively.

He is currently a Lecturer in the Electrical and Electronic Engineering Department at Imperial College London. He was a visiting student at Stanford University, Stanford, CA, in 1996, and, from July to October 2000 he was a Summer Researcher in the Mathematics of Communications Department at Bell Labs, Lucent Technologies. Before joining Imperial College in November 2002, he was a Senior Researcher within the Swiss National Competence Center in Research on Mobile Information and Communication Systems.

His research interests include wavelet theory, approximation and sampling theory, multirate signal processing, and distributed image/ video processing and compression.

Dr Dragotti is currently serving as an Associate Editor of the IEEE Transactions on Image Processing.

Pancham Shukla

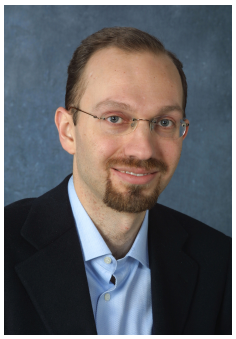

Pier Luigi Dragotti